Fundamentals and Recent Applications of Catalyst Synthesis Using Flame Aerosol Technology

Shuo Liu, Mohammad Moein Mohammadi, Mark T. Swihart*

Department of Chemical and Biological Engineering, University at Buffalo, The State University of New York, Buffalo, NY 14260, USA

*swihart@buffalo.edu

Abstract

Commercial implementation of new catalysts is often limited by scale-up. Flame aerosol processing, a proven scalable method for industrial manufacturing of nanoparticles, has received broad attention for use in catalyst synthesis over the past two decades. This review aims to provide a straightforward understanding of the flame aerosol synthesis of catalysts and summarize recent and emerging applications of the resulting catalysts. We begin with a brief description of the catalyst formation mechanism and show how catalyst structures can be controlled by varying process parameters and reactor configuration. We then summarize the most recent progress on thermal catalysts, photocatalysts, and electrocatalysts synthesized by flame aerosol processing and analyze current trends in catalyst development by this approach. Finally, we discuss the advantages and limitations of flame-made catalysts and suggest likely promising future directions for research in this field.

***Keywords*:** Flame aerosol processing; flame spray pyrolysis; thermal catalysis; photocatalysis; electrocatalysis

1. Introduction

Bridging the gap between laboratory synthesis and industrial production, *i.e.*, achieving scalability, is a persistent challenge in catalyst design and development [1]. Many common laboratory synthesis methods encounter serious barriers to scale-up associated with high manufacturing cost and physicochemical property changes. In contrast, flame aerosol synthesis, the most common technology for industrial production of low-cost nanomaterials [2], provides inherent scalability and flexibility in catalyst design. The first uses of flame-made nanoparticles date back to prehistoric human civilization. Ancient people created carbon black by combustion of plants and used it to draw primitive murals that can still be seen in Chinese, Egyptian, and Indian caves. People in ancient China were the first to produce carbon black in large quantities [3]. In modern times, the development of flame aerosol processing was mostly driven by the industrial production of carbon black, fumed silica (SiO_2), and titania (TiO_2). Carbon black was initially produced by pyrolysis of natural gas in the “channel black” process, but with low efficiency. In 1941, engineers invented flame spray pyrolysis, the “furnace process”, to scalably produce carbon black with controllable particle size, structure, and porosity [4]. Nowadays, this is the dominant process practiced by Cabot, Evonik (formerly Degussa), and others, to make carbon black, the largest nanoparticle commodity by value and volume. Flame aerosol synthesis of fumed SiO_2 was invented by scientists at Degussa who hoped to find another rubber filler to replace carbon black during world war II, but it is mostly used as a flow aid and viscosity modifier [4]. Building on the understanding of fumed SiO_2 production, another famous flame aerosol process, the “chloride process” for the production of pigmentary TiO_2, was created and is still used today by many companies [2]. In fact,

enterprises like Cristal, Cabot, and Evonik produce millions of tons of nanomaterials *via* flame aerosol processing, including carbon black, fumed silica, TiO_2, Al_2O_3, and other ceramic powders [5], and production rates can be scaled to several tons per hour per reactor [6]. Even in the laboratory, flame aerosol processing has enabled large scale fabrication of SiO_2 (up to 1000 g h^{-1}) and ZrO_2 (up to 600 g h^{-1}) with consistent properties [7], of crystalline $Ba_{0.5}Sr_{0.5}Co_{0.8}Fe_{0.2}O_{3-\delta}$ perovskite (up to 400 g h^{-1}) for cathode material [8], and of the binary catalyst V_2O_5/TiO_2 (200 g h^{-1}) for NO removal [9], indicating its scalability for more complex nanomaterials.

Aerosol flame processes are often classified according to the precursor state into vapor-fed aerosol flame synthesis (VAFS) and liquid-fed aerosol flame synthesis (LAFS). Depending on the precursor solution combustion enthalpy, LAFS can be further classified into flame spray pyrolysis (FSP, when a combustible organic precursor supplies more than 50% of the combustion energy) and flame-assisted spray pyrolysis (FASP, when an external flame provides the energy and the precursor is dissolved in water or other solvent with low enthalpy of combustion). VAFS is the most common flame aerosol process in industry. Examples include the earliest “channel black process” to produce carbon black, flame hydrolysis of metal halide vapors to produce fumed silica, and the “chloride process” to produce pigmentary TiO_2 [10]. Later on, VAFS was widely used to synthesize ceramics including Al_2O_3, Fe_2O_3, and V_2O_5 [11]. In catalysis, VAFS has mostly been used for preparing TiO_2-based [12, 13] and Al_2O_3-supported [14] catalysts at the beginning of this century. However, the requirement of using volatile metal precursors increases costs, and achieving homogeneous distributions of elements in multicomponent catalysts with limited precursor selections is challenging. Factors like these have limited its further

development. Liquid-fed reactors overcome these limitations. The use of aqueous metal salt solutions or metal-organic solutions enables the synthesis of materials containing almost every metal in the periodic table [10]. In the FASP process, the precursor is first atomized into small droplets and then sprayed into a flame, evaporated, and pyrolyzed at high temperatures. The first application of FASP was for preparing ZnO particles from a zinc acetate precursor, reported by Marshall et al. in 1971 [15]. Nitrates are the most used precursors in the FASP process. Many catalysts have been synthesized by FASP, particularly various perovskite structures [16-18]. A drawback of FASP for preparing catalysts is its potential to form inhomogeneous and submicron particles, especially at low flame temperature or low precursor feed rate. In the FSP process, the metal-organic precursor solution also serves as a fuel. The resulting short residence time, high flame temperature, and large temperature gradient usually promote the formation of homogeneous, nanoscale, and highly crystalline particles. As a result, FSP has become the primary flame aerosol process for the synthesis of catalysts in recent years. As early as during world war II, the original FSP technology, the “furnace process” to produce carbon black, was developed, and Sokolowski et al. first utilized this method to synthesize Al_2O_3 particles from a benzene solution of aluminum acetylacetonate in 1977 [19]. However, other FSP synthesized nanomaterials were only reported 20 years later. After that, this technology was widely used to produce various nanomaterials, and several scalable FSP reactors gradually appeared [20, 21].

The first flame-aerosol-made catalyst was the TiO_2 photocatalyst reported by Formenti in 1972 [22]. Later, Degussa adopted this technology to produce the P25 TiO_2 photocatalyst, which became the standard material in photocatalysis [23]. However, this work received

little attention in that era because of uncertainty about the mechanism of particle formation. New flame-made catalysts only began to be reported 20 years later [24-26]. Since then, scientists gradually recognized the potential of nanocatalysts synthesized by flame aerosol processing, leading to rapid growth of understanding of particle formation mechanisms and some sophisticated catalysts. Compared to traditional wet chemistry methods, the competitive advantage of flame aerosol processing is the ability to synthesize both the catalytically active species and support in a single-step, continuous process, as shown in **Figure 1**. Wet chemistry methods often require several post-treatment steps, such as solvent washing and calcination, which may introduce changes in catalyst composition and structure as well as impurities and increased cost. In addition, flame aerosol processing gives further flexibility for tailoring catalyst characteristics by controlling process parameters [27], such as precursor feed state (liquid or vapor) [28, 29] and rate [30], flame temperature (solvent combustion enthalpy) [31, 32] and configuration (diffusion or inverse diffusion flame) [33], deposition mode [34], and other parameters, and even forming metastable phases *via* rapid quenching [35-37], which cannot be achieved by wet chemistry methods. Moreover, flame aerosol processing allows active species to nucleate from individual atoms, contributing to high purity [38], high dispersion [39], and thermally stable materials [40]. Some limitations also exist in this method. For example, preparation of porous materials may not be possible, and the use of combustible organic precursor solutions in some methods can increase production costs.

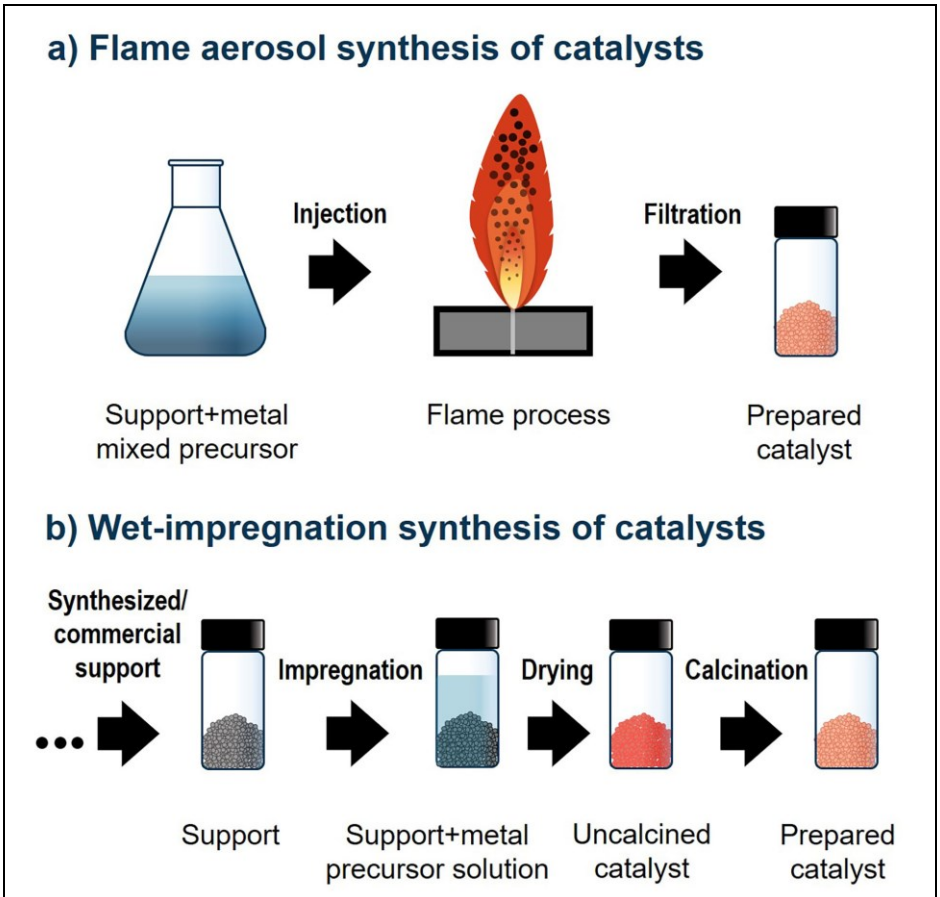

Figure 1. Catalyst synthesis procedures of: **(a)** flame aerosol processing and **(b)** a typical conventional wet impregnation method.

Despite having many advantages for commercial-scale catalyst production, flame aerosol processing has attracted less attention from academic researchers, relative to liquid-phase synthesis methods. This may be because laboratory-scale flame reactors are more difficult to set up and maintain than wet chemistry approaches that may require only basic glassware and an oven. However, it may also reflect limited exposure of the catalysis community to flame aerosol methods. This review aims to introduce and summarize the

emerging applications of flame-aerosol-synthesized nanocatalysts focusing on advances published in the past three years and thereby attract more interest toward this field. Readers interested in further information can refer the review paper by Koirala et al. [41], which provides a holistic view of flame aerosol mechanisms, synthesis conditions and catalyst properties. Reviews of flame-synthesized catalysts published before 2018 are also available [27, 42, 43]. Only flame aerosol synthesis is reported herein; other aerosol processes, like drying, precipitation, high-temperature thermal decomposition, and gas atomization have been well reviewed elsewhere [44].

2. Mechanism and catalyst design

2.1. Particle synthesis mechanism

The development of thermophoretic sampling with microscopy, *in situ* measurements, neutron scattering, and other techniques have revealed particle formation mechanisms in flame aerosol synthesis [45]. Typically, particle formation is believed to proceed by the following steps in turn: precursor evaporation and decomposition → nucleation from a supersaturated vapor or reactive fragments → growth by surface reaction and coalescence → aggregation and agglomeration. Particles formed directly from molecular species are called primary particles and are usually quasi-spherical. Aggregation produces non-spherical, often fractal-like structures made up of these primary particles. FSP and FASP can involve two paths: droplet-to-particle and gas-to-particle conversion, as shown in **Figure 2**.

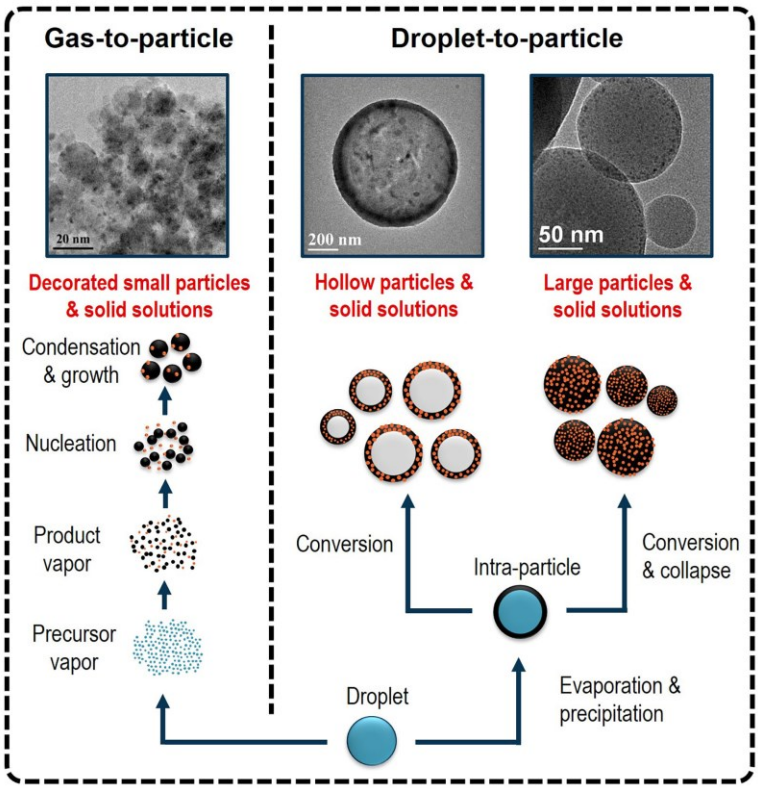

Figure 2. Schematic of particle nucleation and growth mechanisms in FSP or FASP processes. Overall figure adapted from ref. [43] using an image (top left) from [46] with permission from Royal Society of Chemistry and Elsevier, respectively.

In the gas-to-particle path, product molecules nucleate from the gas phase and then grow. The droplet-to-particle conversion mechanism is more common at low temperature or high precursor concentration, or when the size of droplets sprayed into the flame is too large. In this case, primary particles precipitate at the surface of unvaporized precursor droplets. Then the remaining solvent evaporates to form hollow particles, which may collapse and densify to form large particle. When a multi-component precursor mixture goes into a flame aerosol process, the mechanism becomes more complicated, and many

possible particle configurations may be formed, as well described in a previous review paper [10]. For catalyst design, the most desirable structure is usually one in which active components are well dispersed on the support surface [46]. In order to obtain such a structure, the melting point (or sublimation point) of the support should be much higher than that of the active component. With decreasing temperature in the post-flame region, the support with high melting point, such as SiO_2 or Al_2O_3, nucleates and condenses first, and then the active components deposit on its surface. Rapid quenching and short residence time are necessary to form this structure and prevent sintering of the active component, thus maintaining high dispersion.

2.2. Control of Catalyst Structure and Properties

Various reaction parameters in flame aerosol processing play a role in catalyst structure, thereby affecting catalyst performance in the final application. Precursor concentration and feed rate, dispersion gas (oxygen and inert gas) flow rate, solvent/fuel enthalpy, and reactor configuration and size are some of the main parameters that affect catalyst properties. This array of parameters provides infinite flexibility for catalyst design, but also makes catalyst optimization complex. During flame aerosol processing, one can even add some extra means for control of the particle structure, e.g., finer particles can be obtained by N_2 quenching to stop particle growth [47], or an accelerating electric field can be applied to shorten the particle residence time in the flame [11]. **Figure 3** shows a holistic view of the relationship between flame synthesis parameters and catalyst properties. Particle formation mostly depends on the residence time and flame temperature; while the residence time depends on gas flow rate, and flame temperature depends on the solvent/fuel enthalpy and fuel/oxidizer equivalence ratio. The actual relationship is much

more complex than this, and understanding it is vital to the fabrication of nanocatalysts with desirable characteristics and performance.

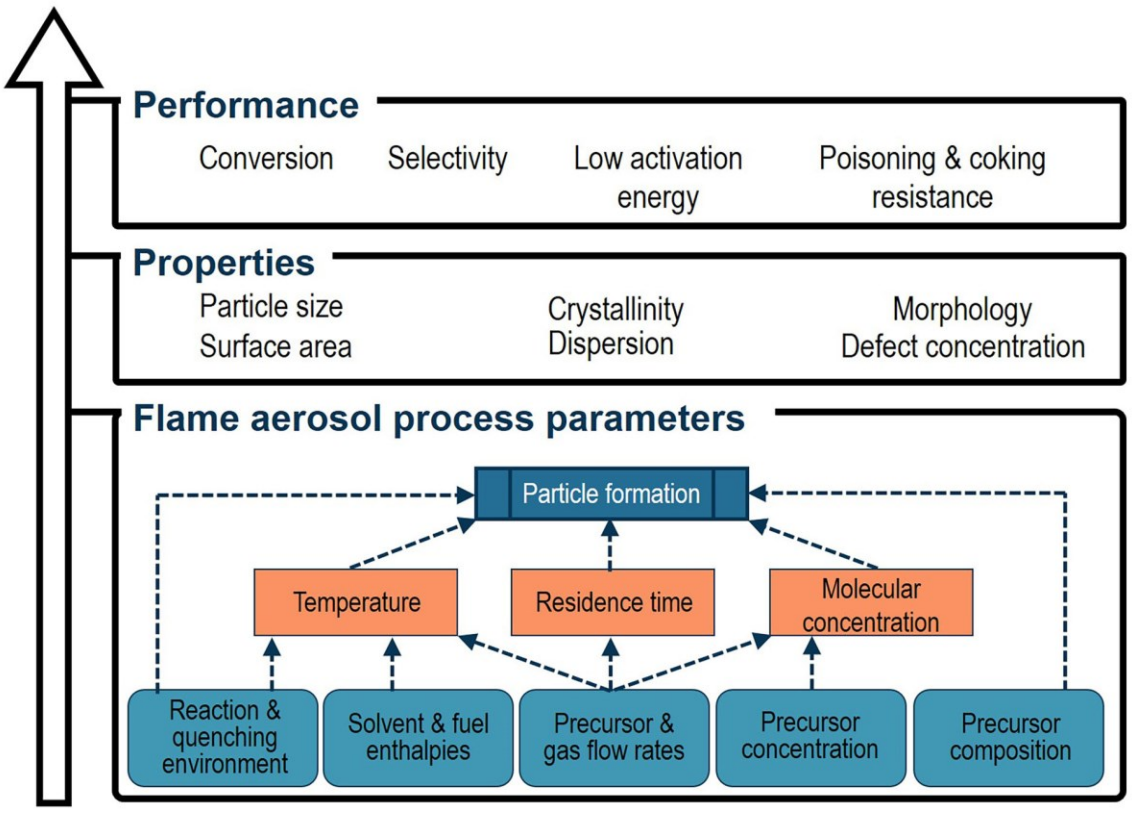

Figure 3. Schematic of process-property-performance relationships for catalyst design and production by flame aerosol processing.

2.2.1 Particle size

Particle size strongly affects catalyst performance; a smaller particle size provides more surface area and active sites. Usually, particle size depends on the molecular concentration, temperature, and residence time during particle formation. Therefore, precursor concentration and feed rate, dispersion gas flow rate, and solvent/fuel enthalpy have decisive effects on particle size. For example, a precursor with a high feed rate and concentration provides high molecular supersaturation in the flame aerosol process, thus

increasing nucleation and coalescence rate and contributing to particle growth. In contrast, a high dispersion gas flow rate could decrease molecular concentration and favor shorter residence time, resulting in smaller particle size. A study of ZrO_2 nanoparticle synthesis [48] considered the effect of precursor concentration, O_2 flow rate, and reactor length on both primary and agglomerate particle size, as shown in **Figure 4a**. At the same conditions, the particle size produced from 1 M Zr precursor was always larger than that produced from 0.5 M precursor solution, and the high oxygen flow rate gave a smaller primary particle size. For 0.5 M Zr precursor, the final primary particle diameter decreased from 13.2 to 7.4 nm when the O_2 flow rate increased from 3 to 7 L min^{-1}, and for 1 M Zr precursor, that particle diameter decreased from 17 to 9.6 nm. The high dispersion gas flow rate reduces primary particle size, but has little effect on agglomerate particle size. The aggregation and sintering of primary particles are mostly influenced by the temperature and the precursor solution concentration.

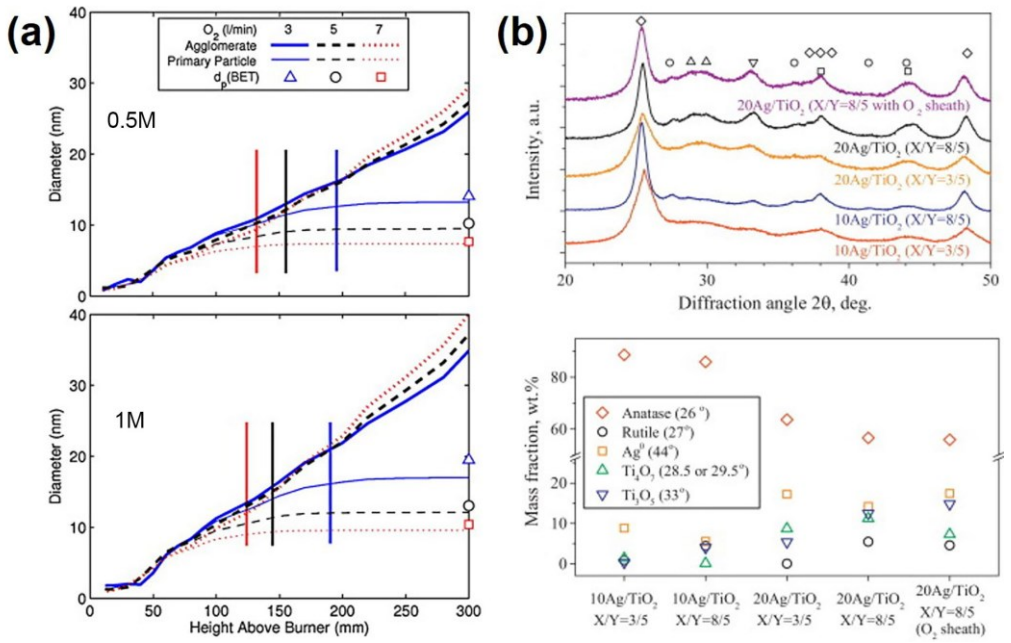

Figure 4. (a) The influence of precursor concentration, O_2 flow rate, and reactor height on FSP-made ZrO_2 particle size. **(b)** XRD patterns of FSP-made Ag/TiO_2 catalyst produced under different conditions, with different phase content in Ag/TiO_2. X: precursor feed rate (ml/min); Y: O_2 feed rate (L/min). Adapted from ref. [48] and [54] with permission from Elsevier.

Along with the process parameters mentioned above, flame configuration must be considered. In a study focused on preparing a TiO_2 photocatalyst, the primary particle size dropped from 70 to 20 nm with use of an inverse diffusion flame in place of a classic diffusion flame [33]. This is because the inverse diffusion flame favors a lower flame temperature, leading to less coalescence and sintering. During thermal catalysis,

maintaining constant particle size is a challenge. The active species may diffuse and sinter at high temperatures, resulting in catalyst deactivation. Flame aerosol made catalysts form from the gas phase, usually above 2000°C, which may lead to inherent thermal stability, often allowing the use of less expensive metals that may otherwise be more prone to sintering than expensive precious metals. For example, FSP-made Ni-based catalysts may replace Pt-based or Ru-based catalysts in methane dry reforming catalysis [49].

2.2.2 Specific surface area

Specific surface area (SSA) is another critical factor for catalyst performance. Effective catalysis requires that reactants have sufficient contact with active sites, so the active species are generally dispersed on some high SSA support to increase the surface-to-volume ratio. Flame aerosol processing generally produces non-porous particles, so the SSA is mostly determined by the primary particle size. Therefore, all of the factors that influence particle size, as discussed above, also affect SSA. For example, in an FSP process, when the precursor concentration increased from 0.05 to 1 M, the primary particle size of SnO_2 increased from 5 to 11 nm, while the SSA decreased from 165 to 75 $m^2\ g^{-1}$ [50]. In an exception, flame aerosol processing occasionally enables the production of nano-silica with considerable SSA, e.g., 500 $m^2\ g^{-1}$ FSP-made Co/SiO_2 catalyst for ethane dehydrogenation has been reported recently [51]. One creative method that combines the aerosol and sol-gel processes, the “aerosol-assisted sol-gel process”, is capable of fabricating porous and advanced catalysts, as shown in **Figure 5**. A solution containing a catalyst precursor and a surfactant is atomized, forming homogeneous droplets that contain inorganic precursor molecules (shown as blue spots) and surfactant

molecules (shown as red spots). Then droplets are dried by mild heating (at a temperature much lower than typical flame aerosol processing temperatures). During the evaporation process, surfactant molecule self-assembly forms micelles, and inorganic polycondensation happens near the micelles, producing inorganic oxide particles surrounding the micelles. Finally, matrix particles are calcined to remove the micelle template and generate porosity [44]. This process can not only synthesize catalysts with high SSA and ordered porous structure, e.g., Zhang et al. synthesized Pd/PMO catalyst (for Barbier reaction with 1674 m^2 g^{-1} SSA, TEM image shown in **Figure 5**) [52], but also provides flexibility for designing catalyst properties by controlling both aerosol and sol-gel parameters. This approach, however, has not yet been coupled with flame aerosol synthesis. Doing so will be challenging, but also represents an open opportunity in the field.

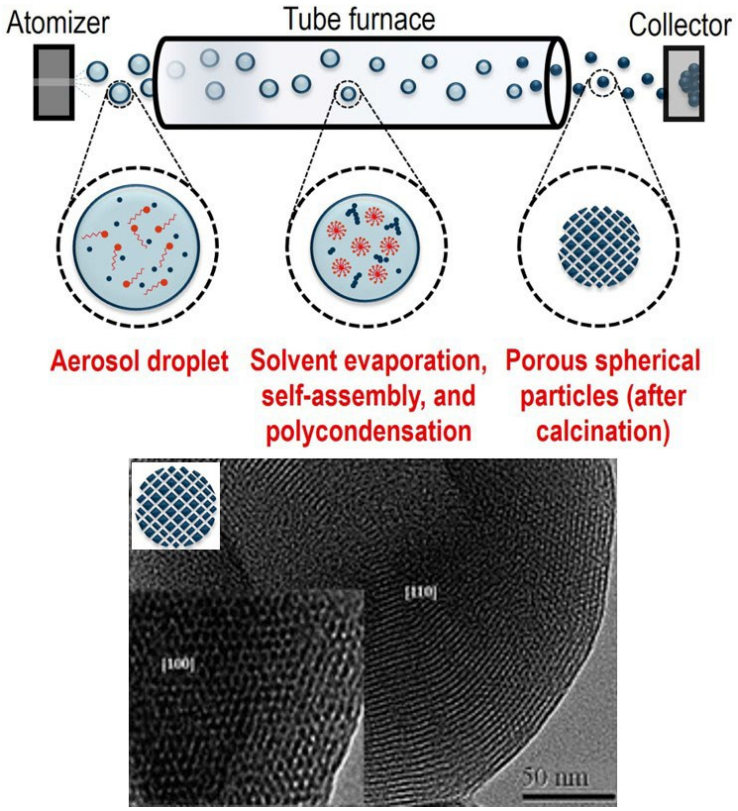

Figure 5. Schematic of the aerosol-assisted sol-gel process for the synthesis of porous particles, and TEM image of high SSA Pd/PMO catalyst prepared by this method. Adapted from ref. [44] and ref. [52] with permission from the Royal Society of Chemistry and Wiley-Blackwell.

2.2.3 Crystallinity and composition

Determining a complete relationship between the crystalline structure and composition of catalyst and its performance is extremely difficult. However, for a given substance, we can sometimes alter the crystal structure and composition by adjusting flame process parameters and/or doping additional elements, with the effect of promoting its catalytic

activity or making it more selective for certain reactions. A typical example is the synthesis of TiO_2 of different phases and compositions. For example, the FSP-synthesized polycrystalline TiO_2 P25 photocatalyst contains approximately 88 wt% anatase and 12 wt% rutile. By decreasing the precursor/dispersion oxygen ratio from 5/5 to 1/5, around 27 wt% monoclinic TiO_2(B) phase and 23 wt% amorphous TiO_2 appeared, resulting in higher photocatalytic efficiency for photocuring epoxy than P25 [53]. Metastable TiO_2 phases can also be formed by rapid quenching. In another study, two metastable phases, Ti_3O_5 and Ti_4O_7, were found in an FSP-made Ag/TiO_2 photocatalyst, which showed higher catalytic performance for the degradation of methylene blue and Cr^{6+} compared to P25 [54]. There, the percentage of different TiO_2 phases could be controlled *via* the precursor fed rate and Ag content, as shown in **Figure 4b**. Also, a diversity of elements have been doped into TiO_2 for the control of catalyst properties. In a study of TiO_2 sensors, Nb-doping promoted anatase phase formation and prevented crystalline growth, while Cu-doping enhanced the transformation of anatase to rutile. Both Cu and Nb doping increased the CO sensitivity of the sensor [55]. However, in another case, Cu and F doping showed less influence on the TiO_2 phase, but they greatly affected the catalytic activity. The F-doped TiO_2 exhibited much higher photocatalytic performance than P25, while Cu-doped TiO_2 exhibited lower activity for oxidation of acetaldehyde [56]. Moreover, studies indicated that N-doping could change the TiO_2 band structure and decrease its band gap, leading to enhanced photocatalytic activity at visible light wavelengths [57, 58]. In addition to these, flame aerosol processing has been applied to the synthesis of various perovskite structures. This area was well described in previous review papers [41, 45].

Apart from the above-mentioned properties, flame aerosol processing also allows the optimization of morphology [59], surface defects [60], and other properties. Generally, as shown in **Figure 3**, flame aerosol design of catalysts follows a route of process parameters → catalyst composition and structure → catalytic performance → application. The numerous flame process parameters provide infinite possibilities for tailoring catalyst structure towards desirable performance and applications.

2.3. Two advanced flame aerosol reactors

Since Bickmore et al. [61] pioneered the gas-assisted atomizer FSP reactor in 1996, flame aerosol processing has been extensively developed, and various flame reactors were invented. For example, Thybo et al. [62] created the one-step deposition flame reactor in 2004, which further promoted supported heterogeneous catalyst and gas sensor preparation; Grass and Stark [63] reported the reducing flame reactor in 2006, making it possible to produce metallic nanoparticles; Teleki et al. [64] developed an *in situ* coating technology by installing a torus pipe ring on an FSP reactor to introduce a coating material. Herein, we present two representative novel flame aerosol reactors, double nozzle flame spray pyrolysis (DFSP) and the high-temperature reducing jet (HTRJ) reactor, which can accomplish flexible catalyst structure design.

2.3.1 Double nozzle flame spray pyrolysis reactor

Strobel et al. first reported the DFSP reactor in 2006 for the preparation of $Pt/Ba/Al_2O_3$ catalysts for NO_x storage and reduction (NSR) [65]. The DFSP reactor used two separate nozzles, one producing the active species precursor and the other producing the support precursor, as shown in **Figure 6a**. The active components and support had independent nucleation and growth processes, and then the two types of particles aggregated, forming

the catalyst structure. Compared to the single nozzle flame reactor, the DFSP reactor provides access to designed particle structures by control of inter-nozzle distance and angle, resulting in unprecedented control of crystallinity and catalytic activity. In the DFSP-made Pt/Ba/Al_2O_3 catalyst, crystalline $BaCO_3$ appeared, whereas it was amorphous when prepared using a single nozzle FSP reactor. Also, the crystalline $BaCO_3$ content increased with increasing inter-nozzle distance [65]. As a result, it exhibited a much higher NO_x storage capacity than single-nozzle-made catalyst. A similar situation was observed for Pd/Al_2O_3 catalyst [66], which also showed higher NO_x catalytic activity than catalysts made by a conventional FSP reactor or a wet chemistry method. The most significant advantage of the DFSP reactor is its ability to produce multicomponent catalysts. In a traditional flame aerosol reactor, when three or more elements are involved, the particle formation mechanism and the possible precursor interactions can become very complex, limiting ability to control the final catalyst structure. The multi-nozzle flame reactor can mitigate such a situation by forming different particles via independent processes. Varying the inter-nozzle distance can allow sufficient residence time for each component to form a desirable structure before mixing, yet still ensure that the components are intimately mixed within aggregates. This approach can also address problems of precursor solution immiscibility, providing more flexibility in catalyst formulation. Therefore, the DFSP reactor became very popular for catalyst design. For example, Fe/Al_2O_3 and Mn/Al_2O_3 catalysts for CO oxidation were synthesized employing both single nozzle and double nozzle reactors. The highest catalytic activity was obtained by the 10 wt% Fe/Al_2O_3 catalyst made *via* the DFSP reactor. It showed more than 30% CO conversion, which was double that of Fe/Al_2O_3 catalyst synthesized in the single

nozzle reactor. The better performance of DFSP-made catalyst was attributed to the prevention of the incorporation of the catalytically active Mn and Fe-species into the alumina support [67]. A similar conclusion was found for a Co-Mo/Al_2O_3 catalyst in which the DFSP synthesis process prevented detrimental $CoAl_2O_4$ phase formation in a hydrodesulfurization catalyst [68]. Pt/FeO_x-CeO_2 catalysts for preferential oxidation of CO were also prepared by a DFSP reactor, which altered interactions between Pt/FeO_x and CeO_2 by increasing inter-nozzle distance. The preferred catalyst structure was obtained at the farthest nozzle distance. This catalyst gave nearly 100% CO conversion at 90°C, a temperature lower than that required for the majority of reported catalysts [69]. These highly active catalysts demonstrate the enormous potential for designing catalyst structure and enhancing catalyst performance *via* the DFSP reactor.

2.3.2 High temperature reducing jet reactor

Another interesting aerosol flame reactor, the high temperature reducing jet (HTRJ) reactor, was developed by Scharmach et al. in 2010 [70], as shown in **Figure 6b**. To date, many multi-component metal nanoparticles, such as Ni-Ag [71], Ni-Cu [47], and Pd-Cu nanoparticles [72], were produced by the HTRJ flame reactor. The HTRJ reactor belongs to the FASP category, using an aqueous inorganic precursor and hydrogen-oxygen flame supplying all of the combustion energy. During the flame synthesis process, the hot gas (N_2, excess H_2, and H_2O from combustion) above the flame enters a thermal nozzle, which can convert part of the combustion enthalpy into kinetic energy of the exiting gas, resulting in a sonic velocity turbulent jet of hot gas. At the same time, the aqueous precursor enters the throat of the nozzle, and is rapidly heated and atomized by the hot gas. The resulting droplets evaporate, the precursor decomposes, and nanoparticles

nucleate, grow, and are finally quenched. Traditional flame-based aerosol reactors often must use high-enthalpy organic solvents for preparing precursors, so the particles form in a flame at very high temperature. A notable characteristic of the HTRJ reactor is that it decouples the combustion chemistry from the particle formation process into different regions of the reactor. This allows the use of low-enthalpy aqueous precursor solutions of inexpensive metal salts. Particles of many transition metals can be reduced by hydrogen in the presence of water vapor, and this decoupling is particularly advantageous for the synthesis of metal nanoparticles that are mildly prone to oxidation. Metals used as supports are generally oxidized by water vapor in the presence of hydrogen. Therefore, the HTRJ reactor is capable of preparing metal active components and oxide supports in one step, without a post-synthesis reduction treatment. This decoupling also allows the use of aqueous metal salt precursor solutions, providing flexibility in catalyst precursor selection, and reducing cost and environmental impact. For example, the HTRJ reactor has recently been used to produce supported nickel-based catalysts for dry reforming of methane using mixtures of nitrate salt precursors for both the support and active metal [73]. These show good dispersion of the metal on the support, as illustrated by the TEM image of HTRJ-made Ni/Al_2O_3 catalyst in **Figure 6b**. More importantly, the HTRJ reactor allows particle formation to happen at a relatively low temperature (500~700°C) compared to traditional reactors (above 2000°C), due to the decoupling of particle formation from the flame, cooling that takes place across the nozzle expansion, and the use of aqueous precursors with high specific heat and heat of vaporization. Additionally, the particle formation temperature can be further lowered by altering flame position and oxygen flow rate. This method also provides a great opportunity for the synthesis of carbon-supported metal structures [74], which have application potential in electrocatalysis.

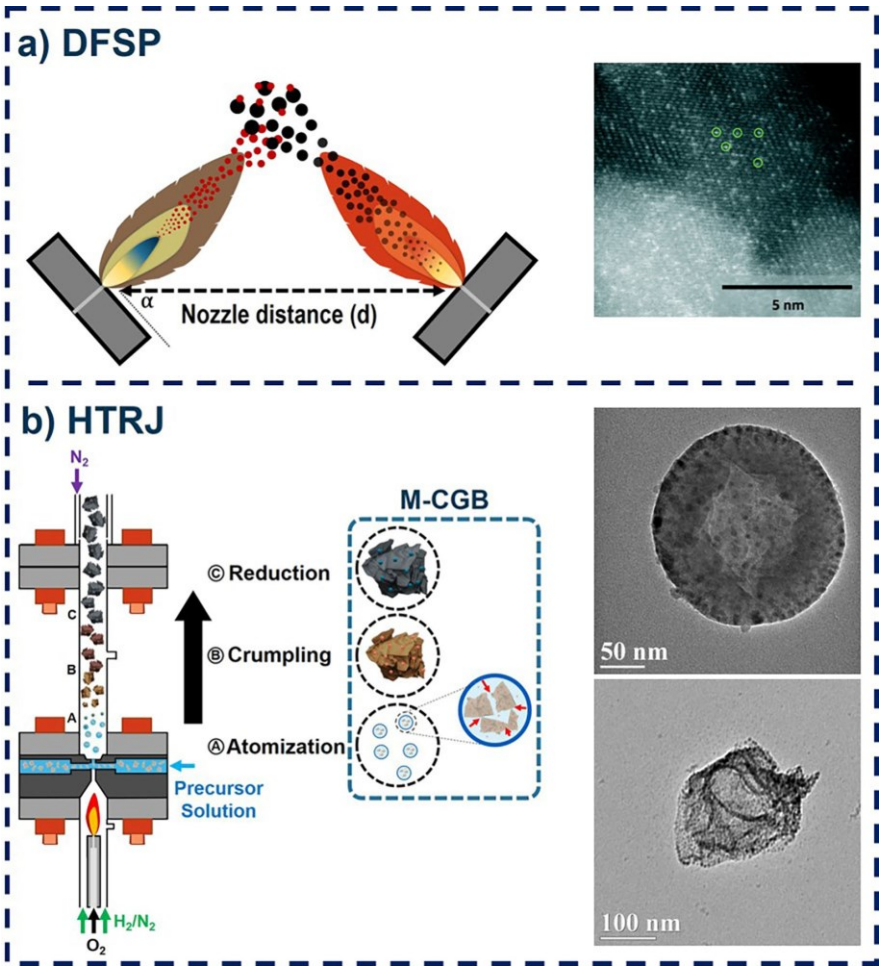

Figure 6. (a) Schematic of DFSP reactor and HAADF image of La-Co/Al_2O_3 catalyst prepared by it. **(b)** Schematic of HTRJ reactor (left), schematic mechanism of formation of metal-decorated crumpled RGO (center), and TEM images (right) of Ni/Al_2O_3 catalyst (top-right) and graphene-supported CoNi (50:50 wt%, bottom-right) structures. Adapted from ref. [82] and [74] with permission from Royal Society of Chemistry.

3. Recent applications in thermal catalysis

The previous sections provided an overview of flame aerosol synthesis of catalysts, concisely describing the historical development and the particle formation mechanisms of flame aerosol processing, as well as the effect of process parameters and reactor configurations on catalytic properties. The following two sections provide a critical summary of the most recent flame-made thermal catalysts, photocatalysts, and electrocatalysts, aiming to reveal current research trends and predict future directions. For thermal catalysis, the high thermal stability of flame-synthesized catalysts enable stable catalytic activity at high temperatures. **Table 1** summarizes thermal catalysts fabricated *via* flame aerosol processing and reported over the past three years. These studies mostly focus on environmental and energy issues. Reactions such as CO_2 reduction, methane reforming, and CO removal have garnered the most attention. This chapter divides these thermal catalytic reactions into CO_2 utilization, harmful gas removal, and organic synthesis processes and describes them separately.

3.1 CO_2 utilization

The 2015 Paris Climate Agreement calls for limiting global warming to a rise of 1.5~2 °C [75]. Thus, in recent years, energy and environmental issues related to control of CO_2 emission and clean use of fossil fuels are increasingly urgent. Some promising thermal catalytic reactions for CO_2 utilization, such as CO_2 methanation ($CO_2 + 4H_2 \rightarrow CH_4 + 2H_2O$) and dry reforming of methane (DRM, $CH_4 + CO_2 \rightleftharpoons 2CO + 2H_2$) are of increasing interest in both scientific and industrial contexts. The development of high performance, economical, and durable catalysts has become a core challenge for large-scale implementation of such processes. Even though some related catalysts [39, 76] had been

produced by the FSP method several years ago, research in this area remains very active. For CO_2 hydrogenation, many byproducts are involved, so the selectivity to the main product is important. Dreyer et al. [77] recently synthesized Ru-based CO_2 methanation catalysts by the FSP process that were able to attain as high as 99% methane selectivity. This study explored the influence of four oxide supports (Ru/CeO_2, Ru/MnO_x, Ru/Al_2O_3, and Ru/ZnO) and their reducibility on the CO_2 methanation activity. In Ru-based catalysts, oxide supports supply CO adsorption sites while Ru provides H_2 dissociation sites, and both of them determine the CO_2 conversion and selectivity. Among these four catalysts, the Ru/Al_2O_3 combination exhibited the highest Ru-CO coverage, followed by Ru/CeO_2, Ru/MnO_x, and Ru/ZnO; however, too much Ru-CO coverage would decrease the number of H_2 dissociation sites. Therefore, the mild reducibility of Ru/CeO_2 catalyst provided the optimal CO adsorption situation, not only achieving high CO coverage but also retaining enough H_2 dissociation sites, leading to the highest catalytic performance.

Besides CO_2 methanation, CO_2 hydrogenation to methanol also received attention. All of the recent flame-made catalysts for this reaction were Cu/ZrO_2. For example, Tada and Fujiwara et al. studied the influences of Cu loading [78], particle size and crystallinity [79] on catalytic performance. The Cu loading varied from 20% to 80%. Low loading benefits Cu dispersion and interaction with ZrO_2, while high loading produces more active sites. The optimal catalytic performance was achieved at 60 wt% loading, which combined the advantages of both high Cu dispersion and active site numbers. Cu content also had a significant effect on particle size, which increased from 10 to 20 nm with increasing Cu content. Another influencing factor for particle size is the precursor feed rate. Upon increasing the feed rate from 1 to 10 mL min^{-1}, the Cu particle size dropped from 17 to 12

nm. However, particle size was not the decisive factor for catalytic performance and the best performance (as shown in **Table 1**) was achieved by catalysts produced at a relatively low precursor feed rate (3 mL min^{-1}), because of its impact on the support crystal structure. Usually, ZrO_2 exists in a tetragonal crystalline structure, but at low feed rate, a substantial fraction of amorphous ZrO_2 was produced, resulting in weak adsorption of methanol onto the catalyst surface and suppressing methanol decomposition to CO. Compared to the CO_2 methylation catalysts prepared by wet chemistry methods, the particle size of the flame-synthesized Cu/ZrO_2 catalysts were smaller. Tada et al. [80] further improved the structure and performance of Cu/ZrO_2 catalysts by using a two-nozzle FSP reactor. The two-nozzle reactor provided flexibility for tuning product structure. In this way, the Cu size was below 5 nm, resulting in better dispersion and catalytic activity, and methanol selectivity was higher than that of the commercial $CuO/ZnO/Al_2O_3$ catalysts used for methanol synthesis from syngas.

Dry reforming of methane (DRM) uses two greenhouse gases (methane and CO_2) to produce syngas. Compared to breaking weak H-H bonds in CO_2 hydrogenation, the DRM reaction requires breaking stronger C-H bonds, which in turn requires a high reaction temperature and catalysts that are stable at that temperature. The excellent thermal stability of catalysts synthesized by FSP meets this requirement. Noble metal catalysts show high catalytic performance and excellent coking resistance, but recent studies have focused on transition-metal-based catalysts to reduce cost. An example is the Co/Al_2O_3 catalyst synthesized by Horlyck et al., who investigated the effect of metal-support interactions by varying Co:Al ratio [81]. At 10% Co loading, a strong interaction between Co and Al led to the formation of the spinel phase ($CoAl_2O_4$), which resulted in very limited

Co reducibility and thus rendered the catalyst inactive. Such a situation could be solved by loading more Co. Increasing Co loading to 30% prevented spinel formation, and the readily-reduced Co active sites were well dispersed on the support surface. Also, the deposited Co showed a high basicity, which increased the CO_2 adsorption capacity and the resistance to carbon deposition. Further increasing the Co fraction increased the size of Co deposited on the Al_2O_3 surface and made the catalyst more easily deactivated. Some studies found that doping La into the Al_2O_3 support can also prevent spinel formation and enhance catalytic activity [82, 83]. Horlyck et al. [82] reported that doping 15% La promoted the formation of Co_3O_4 to inhibit the undesirable spinel phase and enhance catalyst basicity, which gave rise to higher CO_2 adsorption capacity and catalytic activity, and reduced catalyst carbonization. The low La loadings resulted in the substitution of single La^{3+} ions into the Al_2O_3 lattice; while aggregated La atoms appeared as crystal defects when the La loading increased. The dispersion of La on the Al_2O_3 was high because La was doped *via* substitution rather than surface deposition. Adjusting the distance between the two nozzles in the DFSP reactor also limited spinel formation and facilitated the production of readily-reduced Co species. Because of these advantages, the La-doped catalyst achieved superior methane conversion (90% conversion at 750°C and 96% at 800°C) compared to prior studies, and the outstanding methane conversion was maintained for at least 24 h, as shown in **Figure 7a**. Generally, metal oxides synthesized in a flame are non-porous, but FSP-synthesized silica can have a much higher surface area than most other flame-made powders [84, 85]. Part of the reason is simply the low density of silica compared to metal oxides, which increases specific surface area for given particle size and structure. In addition, surface area is increased

when a high concentration of nuclei form, and do not sinter. One interesting study utilized an asymmetric DFSP reactor to prepare a high surface area SiO_2-$Ce_{0.7}Zr_{0.3}O_2$ composite support, with one nozzle for preparing silica, the other for $Ce_{0.7}Zr_{0.3}O_2$. This study indicated that during the silica particle formation process, incorporation of 5% “CeZr impurities” can provide isolated sites for silica nucleation and growth, which results in a larger number of smaller silica particles, and thus increases the surface area from 324 to 481 m^2/g relative to undoped silica. [86] Then, the Ni catalyst was loaded on the high surface area support by wet impregnation. This complex Ni-based catalyst had excellent thermal stability, and the preferential deposition of Ni on the silica surface promoted methane decomposition. However, the deposition of Ni on silica supports can lead to the formation of filamentous carbon that causes catalyst deactivation. Thus, although a diverse array of novel structures was achieved by this method, we do not recommend it based on efficiency and economic considerations. These catalysts failed to show a high catalytic performance compared with others fabricated from single impregnation or flame aerosol methods, so the additional steps and associated high cost cannot be justified.

3.2 Harmful gas removal

Harmful gas treatment is another prevalent environmental issue that can be addressed using flame-made catalysts. In this field, most of the recent studies focus on CO oxidation. Unlike CO_2 oxidation, CO oxidation involves very few side reactions and happens at a relatively low temperature, so it has many practical applications in purification and separation, like treatment of automotive exhaust and removal of trace CO from H_2 for use in fuel cells. For these uses, achieving high CO conversion at low temperature is crucial. Ogel et al. prepared Pt/Al_2O_3 catalysts *via* incipient wetness impregnation, FSP,

supercritical fluid reactive deposition, and pulsed laser ablation methods, finding that FSP-made Pt/Al_2O_3 catalyst provided the best catalytic activity and hydrothermal aging resistance [87]. They attributed the excellent performance to the appropriate particle size, indicating that FSP achieved the optimal Pt particle size of 2~3 nm for CO oxidation. Smaller catalyst particles are expected to be highly mobile and thus deactivate during the reaction. However, a different conclusion was reached by Zhao et al. [88], who argued that smaller Pt particles often mean more active sites, contributing to the elevated activity. By doping 1% Co into Pt/TiO_2 catalyst, the Pt particle size decreased from 2.47 to 0.72 nm, reducing the temperature for complete CO conversion from 120 to 70°C. Additionally, increased surface adsorbed oxygen also contributed to the high catalytic activity of Co-doped Pt/TiO_2 catalyst. Surface adsorbed oxygen can form a bicarbonate intermediate, which more easily decomposes to CO_2 than other intermediate products. The Co species on the surface serve as oxygen binding or reservoir sites during the reaction process. Another related study indicated that doping 0.55% N into Pt/TiO_2 catalyst could improve its thermal stability [89]. Nitrogen was introduced *via* a second nozzle and formed Pt-N bonds, which inhibited the movement and aggregation of Pt particles. However, both Co and N dopants promoted the formation of rutile rather than the anatase phase, which is detrimental to the catalytic activity [88, 89].

Compared to Pt-based catalysts, more attention has focused on non-noble metal catalysts for CO oxidation recently because of their low cost and easily tunable activity. For example, a CuO/TiO_2 [90] catalyst synthesized by the FSP process showed complete CO conversion at 120°C, which was comparable to some noble metal catalysts. Meanwhile, Zhao et al. indicated that doping Mn into CuO/CeO_2 catalysts could produce

a synergetic effect to enhance catalytic activity [60]. The CO oxidation reaction starts with CO chemisorption at the CuO-CeO_2 interface to form Cu^+–CO carbonyls that react with absorbed oxygen to form the carbon intermediates. The redox reaction of Mn with Cu ($Cu^{2+} + Mn^{3+} \rightarrow Cu^+ + Mn^{4+}$) generated more Cu^+ species and thus more CO adsorption sites. Moreover, Mn doping provided more oxygen defects and thereby generated more absorbed oxygen. Such synergetic effects enhance CO and O adsorption to improve catalytic performance. In this way, the temperature to reach 90% CO conversion dropped from 200 to 131°C upon doping with Mn. However, contrasting results were presented in another report on a CuO/CeO_2 catalyst [91], which showed excellent catalytic performance by only adjusting Cu loading, achieving 100% CO conversion at only 120°C without any additional doping. CO oxidation catalysts must survive in a humid environment, but many catalysts suffer from rapid hydrothermal deactivation. Flame aerosol processing generally produces catalysts with high moisture tolerance. The previously described CuO/CeO_2 catalysts show low water sensitivity and are suitable to work in a humid atmosphere. Flame-made hopcalite (Cu-Mn oxide) catalysts also showed competitive stability against moisture that was much better than commercial hopcalites [92, 93]. Under humid conditions, water adsorption promotes CO_2 adsorption by dissolution mechanisms, and the subsequent formation of HCO_3^- and CO_3^{2-} that coordinate to Cu^{2+}, thereby causing deactivation. The studies of hopcalites found that, by controlling precursor composition and concentration, gas flow, solvent, and other parameters, the flame aerosol processing could form a 2 to 5 nm thick amorphous carbon layer (TEM image shows in **Figure 7b**) around hopcalite particles, which made the particles hydrophobic. This hydrophobization alleviated the water-based deactivation

mechanism and allowed the catalyst to achieve 50% higher CO conversion than commercial catalysts under humid conditions.

Some perovskite catalysts were also prepared for the removal of harmful gases [94, 95]. Although they failed to give a high CO conversion at low temperatures, some of them could be used for three-way catalysis that deals with CO, NO, and C_xH_y together, as is needed to purify automotive exhaust gas. Apart from CO oxidation, promising catalysts for other reactions of harmful gases, such as NO oxidation [87] and methane combustion [96], were also fabricated *via* flame aerosol processing in recent years. We highlight here one study on FSP synthesis of CuO/TiO_2 nanocatalyst for low-temperature removal of toluene (**Figure 7c** and **7d**), which accomplished up to 90% toluene conversion at temperatures as low as 200°C [97]. This impressive catalyst performance was attributed to the unique advantages and flexibility of FSP. For the dispersion of Cu species on a support, traditional wet-chemistry methods can reach 5~12 wt% loading [98]. However, with particle nucleation from gas-phase atoms, this flame-made catalyst could achieve 20 wt% Cu loading and still maintain very high dispersion. Most of the Cu species were embedded internally, producing more oxygen vacancies, which benefits oxygen adsorption and formation of mobile oxygen species at the metal/oxide interface. Meanwhile, the high reducibility of active sites and the anatase-to-rutile transformation during the FSP process also led to higher catalytic activity. Additionally, the synthesized CuO/TiO_2 catalysts showed good hydrothermal stability, making them suitable for application in many practical situations, such as removal of harmful gases in vehicle exhaust, self-cleaning and air-cleaning (photo)catalytic paints and surface treatments, and biomass utilization.

3.3 Organic synthesis

Besides environmental and fuel-related applications, flame aerosol processing has also produced heterogeneous catalysts for some important organic synthesis reactions in the chemical industry. For example, Wang et al. synthesized high acidity Ru/SiO_2-Al_2O_3 catalysts for the Fischer-Tropsch process. By simply adjusting the ratio of SiO_2 to Al_2O_3, the carbon chain length and the composition of final products could be tuned [99]. Sprenger et al. prepared Bi-Mo-Fe-Co oxide quaternary catalysts for propylene oxidation to acrolein and acrylic acid, showing the great potential of flame aerosol processing for the fabrication of complex catalysts [100]. Pongthawornsakun et al. employed a two-nozzle FSP reactor to produce an $Au-Pd/TiO_2$ catalyst for acetylene hydrogenation, which had much higher catalytic activity (46% C_2H_2 conversion) than catalysts made by conventional co-impregnation (22% C_2H_2 conversion) and deposition-precipitation (19% C_2H_2 conversion) methods [101]. Gavila et al. fabricated a Co-Al spinel catalyst for furfural hydrogenation that showed considerable potential to replace noble metal catalysts [102]. Here, we further consider the FSP-made amorphous silica-alumina and amorphous silica-alumina-phosphate solid acid catalysts for aqueous conversion of glucose to levulinic acid [103]. During the silica-alumina synthesis, by controlling the Si-Al ratio (Al content varied from 0 to 100 mol%), the SSA varied from 180 to 407 m^2g^{-1}, reaching a maximum at 20 mol% Al addition. The SSA continually increased up to 478 $m^2\ g^{-1}$ upon reducing the liquid precursor feed flow rate, demonstrating the flame aerosol synthesis of high SSA catalysts, as shown in **Figure 7e** and **7f**. Benefitting from the high SSA, up to 40% levulinic acid yield was obtained, which was double that achieved by protonated ZSM-5 and zeolite X catalysts. Also, though the addition of phosphate into this system produced an obvious

decrease in SSA, it could greatly increase the amount and strength of surface acid sites, contributing to slightly higher catalytic activity.

Generally, in the past three years, the vast majority of flame-made catalysts have focused on environmental and energy fields. The unique particle formation mechanism of flame aerosol processing provides many valuable characteristics to heterogeneous catalysts, such as high thermal stability, good active component dispersion, and abundant oxygen defects in the support. The tunable flame parameters further contribute to the tailoring of desired structures to deal with moisture, high temperature, or other demanding conditions. In the future, considering the growing demands for controlling carbon emission and treating vehicle exhaust, we believe that CO_2 reduction and CO oxidation reactions will remain areas of concentrated research activity for flame-made catalysts. Notably, with the promotion of the Shale Revolution in North America, as well as China's breakthrough in combustible ice mining technology, methane dry and steam reforming reactions will continue to garner attention.

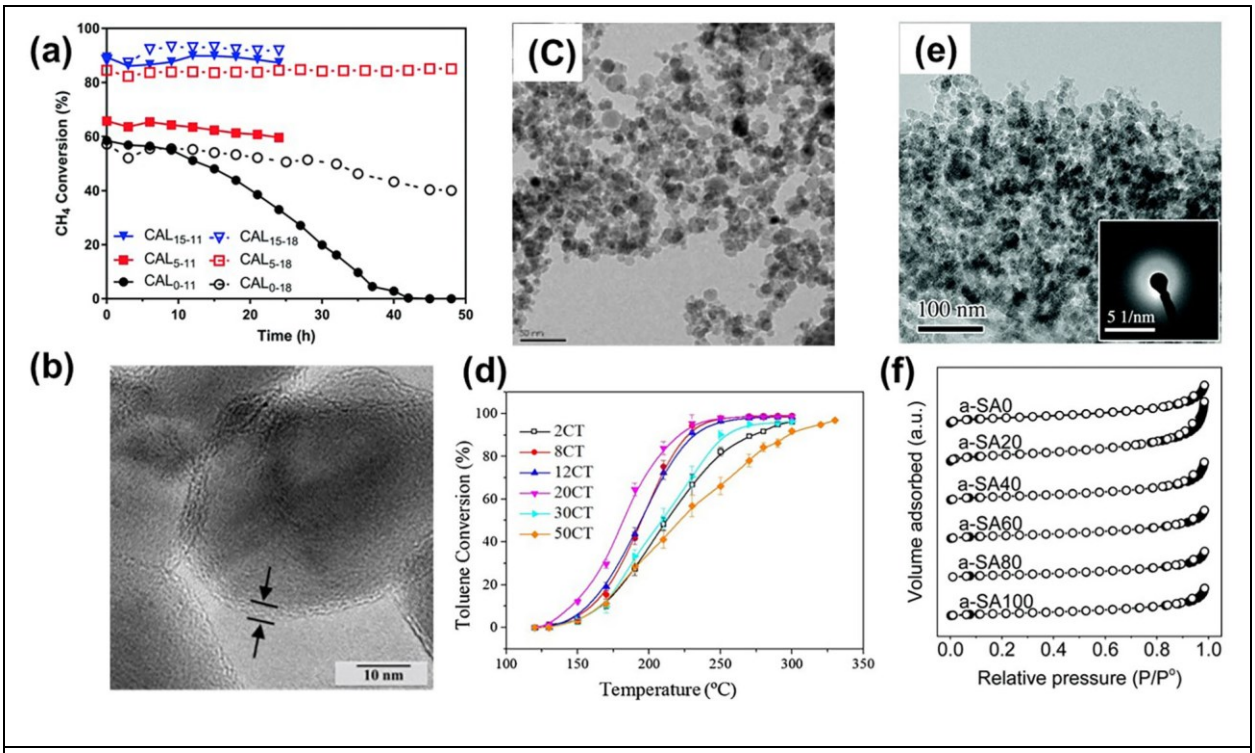

Figure 7. (a) Methane conversions of La-doped Co/Al_2O_3 DRM catalyst at 700°C. In CAL_{x-y}, x is the La content (wt%) and y is the nozzle distance; **(b)** TEM image of amorphous carbon layer around a hopcalite particle; **(c)** TEM image of highly loaded CuO/TiO_2 catalyst and **(d)** its toluene conversion. In xCT, x is the CuO content (wt%); **(e)** TEM image and **(f)** Type II N_2 adsorption-desorption isotherms of high SSA amorphous SiO_2-Al_2O_3 catalyst. Reproduced from ref. [82], [92], [97], and [103] with permission from the Royal Society of Chemistry, European Chemical Societies and Elsevier.

4. Recent applications in photocatalysis and electrocatalysis

4.1 Photocatalysis

Utilization of solar energy to drive reactions *via* photocatalysis has long been regarded as an environmentally friendly and sustainable strategy for producing renewable fuels. TiO_2

is recognized as the most promising photocatalyst due to its activity and stable physicochemical properties. With simple and continuous synthesis steps, flame aerosol processing has become the most common method for large-scale production of TiO_2 photocatalysts in the chemical industry, e.g., the P25 TiO_2 photocatalyst made by Degussa (now Evonik). Furthermore, flame aerosol processing can flexibly adjust TiO_2 structure to meet different reaction requirements. An example of this goal is the control of phase composition to accomplish the best synergistic effect between anatase and rutile for methanol deoxygenation. By adjusting H_2 flow, the anatase content was varied from 4 mol% to 95 mol%, and the optimal catalytic activity was achieved at 39 mol% anatase content [104]. However, the wide bandgap of TiO_2 limits its ability to absorb visible light. So recently, as shown in **Table 2**, most research focuses on co-catalysts that incorporate noble metals, transition metals, or non-metallic elements to narrow its bandgap and enable it to absorb visible light.

Noble metal co-catalysts may improve TiO_2 photocatalytic activity by reducing its effective bandgap, providing new active sites, creating localized surface plasmon resonances, and other effects. For example, Bahadori et al. incorporated Ag in TiO_2 and obtained 1.5 times the NO_3^- conversion for nitrate reduction compared to bare TiO_2 [105]. Recent studies indicated that flame aerosol processing is able to deposit very tiny noble metal particles on the TiO_2 surface, resulting in promising activity and poisoning resistance. In the case of a Pt-TiO_2 photocatalyst for the steam reforming of methanol, the FSP-made co-catalyst exhibited many sub-nanometer Pt clusters (particle size < 2 nm) on the TiO_2 surface [106]. The Pt clusters not only provided more active sites, but also tended to locate on the corners or edges of TiO_2, leading to better dispersion and stronger CO adsorption ability.

Also, reducing the Pt size from nanoparticles to clusters accelerated the methanol and water adsorption kinetics, leading to a high turnover frequency, and hindering the detrimental formation of irreversibly adsorbed CO on Pt. All of these aspects increased the photocatalytic performance of Pt cluster-decorated TiO_2. Furthermore, a flame aerosol process was even able to deposit single Pd atoms on TiO_2 (**Figure 8a**), which produced a four-fold increase in NO_x removal efficiency with respect to bare TiO_2 photocatalyst [107]. The Pd doped in TiO_2 can be divided into four parts, isolated Pd atoms, Pd sub-nanoscale clusters, Pd nanoparticles, and Pd incorporated in bulk TiO_2. As quantified by diffuse reflectance infrared Fourier transform spectroscopy, initially the proportion of isolated Pd atoms increased linearly with increasing total Pd content, and reached a plateau value of 0.055% of the total Pd content, for 0.1 wt% total Pd content. Further increasing Pd content did not produce more isolated Pd atoms due to the formation of Pd clusters. Although the number of isolated Pd atoms was tiny, its effect on photocatalytic activity was decisive. This study indicated that the average NO removal efficiency linearly increased with the fraction of isolated Pd atoms, and the Pd-TiO_2 co-catalyst doped with 0.1 wt% and 1 wt% Pd had similar catalytic performance, indicating the minor role of Pd clusters, Pd nanoparticles, and Pd dispersed in bulk TiO_2. The surprising activity of single Pd atoms suggests that they provide exceptionally active sites for the photocatalytic NO removal, that they are highly selective for NO conversion to nitrate, and that they have high resistance to nitrate poisoning. In total, the flame aerosol processing contributed to the deposition of single Pd atoms onto the TiO_2 surface, maximizing catalyst performance while minimizing the noble metal use.

Doping with other metals can also reduce the TiO_2 bandgap and/or induce charge trapping sites. By doping Ce into TiO_2, the bandgap of TiO_2 was reduced from 3.06 to 2.43 eV, which enabled strong visible light absorption. This light absorption wavelength redshift was attributed to the fact that the 4f orbital energy level of Ce was below the TiO_2 conduction band, so the electrons in the Ce–TiO_2 valence band can be excited into the Ce 4f energy level by visible light. Meanwhile, Ce trapped electrons and inhibited electron-hole recombination, increasing superoxide anion radical and hydroxyl radical generation. In this way, methylene blue photo-degradation efficiency increased from 20% to 70% with respect to bare TiO_2 [108]. On the other hand, the addition of a transition metal does not necessarily enhance photocatalytic performance. The outcome depends on its interaction with TiO_2. For example, Cu doped into TiO_2 could adopt two valence states, Cu^+ and Cu^{2+}. Though both of them could narrow the TiO_2 bandgap, for water splitting hydrogen production, Cu^+ could accelerate the electron-hole separation to promote the photocatalytic reaction. However, electrons on the Cu^{2+} do not have sufficient redox potential to reduce H^+, thus producing an inhibition effect [109]. Flame aerosol processing is conducive to engineering the Cu valence to maximize catalytic activity [110]. By controlling precursor composition and oxidant/fuel ratio, up to 93% surface Cu_2O nanocluster content was achieved, leading to a photocatalytic water splitting rate 22 times higher than P25.

Doping of non-metal elements has long been seen as the third-generation method for modification of TiO_2 photocatalyst properties. It can narrow the TiO_2 bandgap to produce more photogenerated electrons and holes under solar illumination. The addition of non-metal elements by wet-chemistry generally involves large volumes of solvents and

requires several post-treatment steps, making it even more complicated than doping with metals. However, recent studies show that flame aerosol processing enables the synthesis of non-metal doped TiO_2 in a rapid single-step process. For example, S-doped TiO_2 particles can be easily formed during FSP by adding aqueous H_2SO_4 into the TiO_2 precursor [111]. As shown in **Figure 8b**, there is an increase in visible light absorbance with increasing S content in TiO_2. The S atoms incorporated into the TiO_2 lattice mainly existed in S^{6+} and S^{4+} cation states. The presence of S^{6+} reduced the TiO_2 bandgap energy to 2.78 eV and thereby shifted the optical absorption to the visible region. Additionally, S^{6+} and S^{4+} served as electron capture sites and increased the electrical conductivity of TiO_2. A similar method was used to prepare an N-doped TiO_2 photocatalyst by the addition of HNO_3 and urea into the TiO_2 precursor [58, 112]. Most of the N atoms occupied interstitial positions in the TiO_2 lattice, forming Ti-O-N bonds rather than substitutional nitrogen. The interstitial N atoms changed the electronic band structure of TiO_2, resulting in a new N 2p energy band formed above the O 2p valence band, which narrowed the TiO_2 bandgap to 2.47 eV. Also, the interstitial nitrogen atoms inhibited the recombination of the photogenerated electron-hole pairs. Thus, electrons accumulated on the catalyst surface and combined with oxygen, producing highly oxidative species, such as hydroxyl radicals. The highly oxidative species contribute to the degradation of organics. The drawback of this process is that the aqueous dopant precursor would reduce the combustion enthalpy during FSP, leading to a substantial increase in particle size and decrease in surface area. Despite this, both the S-doped and N-doped TiO_2 catalysts showed excellent photocatalytic activity for the degradation of organic pollutants.

Apart from TiO_2, flame aerosol processing also contribute to the synthesis of other photocatalyst materials, such as MoO_3 [113] for hydrogen production and WO_3 [114] for the degradation of organic dyes. A recent study focused on the flame synthesis of a novel torus-shaped g-C_3N_4 photocatalyst due to its moderate bandgap and stable physicochemical properties [59]. An SEM image of flame-made torus g-C_3N_4 is shown in **Figure 8c**. The unusual shape of the g-C_3N_4 was a result of droplet deformation and was influenced by various flame parameters. Generally, high precursor flow rate and temperature caused the droplets' structural instability. Under such conditions, and at a suitable precursor concentration, hydrodynamic processes during solvent evaporation and resulting concentration of solids at the peripheral regions of the droplet finally led to droplet collapse that produced the novel torus shape. Interestingly, the flame process failed to have any effect on the chemical bonding in the g-C_3N_4 network, but reduced surface functional group defects. Sometimes, the surface defects on g-C_3N_4 might inhibit charge transport and/or act as electron-hole recombination centers, which degrade photocatalytic performance. Therefore, the reduction of surface defects led to a significant improvement in photocatalytic hydrogen production efficiency. Moreover, the novel torus-shaped g-C_3N_4 catalyst showed considerable stability, maintaining constant photocatalytic activity for 12 h.

In total, many recent studies focused on doping a second component in TiO_2, to narrow the bandgap, provide new photoactive sites, and produce more photoexcited electron-hole pairs. Flame aerosol processing helps to simplify doping steps and flexibly design co-catalyst composition, structure, and morphology to maximize their synergistic effect. Particularly, it provides the possibility to form isolated Pd atoms on the TiO_2 surface, which

showed amazing photocatalytic activity. We believe that studies on how to design flame parameters to produce more isolated noble-metal atoms are a promising direction for research in the future. Moreover, environmental and energy applications, such as photocatalytic degradation of organic pollutants and water-splitting to produce hydrogen, will remain important topics of research for the foreseeable future.

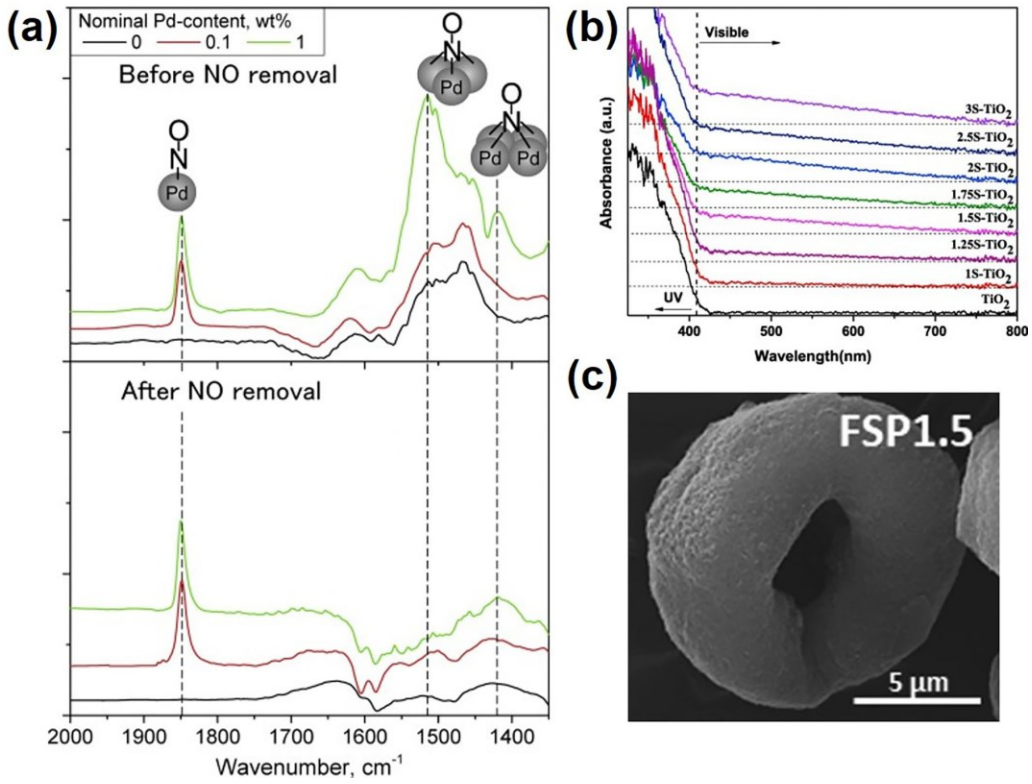

Figure 8. (a) DRIFT spectra of FSP-made Pd/TiO_2 photocatalyst for NO_x removal. The DRIFT peaks at 1847cm^{-1}, 1510 cm^{-1}, and 1420 cm^{-1} represent isolated Pd atoms, Pd sub-nanoscale clusters, and Pd nanoparticles respectively; **(b)** UV–vis diffuse reflectance spectra of S doped TiO_2 photocatalysts with varying S concentrations; **(c)** SEM image of FSP-made novel torus g-C_3N_4 photocatalyst. Reproduced from ref. [107], [111], and [59] with permission from Elsevier.

4.2 Electrocatalysis

Electrocatalysts play an important role in energy conversion and storage devices, such as fuel cells [115] and water-splitting devices [116], but have often been limited by expensive fabrication costs and low production rates. Flame aerosol processing gives access to scalable production of electrocatalysts and allows one to easily tailor the electronic structure by tuning processing parameters. Therefore, even though very few studies have reported the flame aerosol synthesis of electrocatalysts to date, we believe that this field holds great potential for both basic research and practical applications. In a recent study, Daiyan et al. [117] synthesized a ZnO nano-electrocatalyst *via* a FSP process for the production of H_2 and CO (syngas) from water and CO_2, demonstrating unprecedented stability and reactivity with a current density of 40 mA cm^{-2} at an applied cell voltage of 2.6 V (**Figure 9a**), for up to 18 h of CO_2 reduction reaction (CO_2RR). The high CO_2RR activity was attributed to abundant oxygen defects, caused by the fast growth and crystallization process during FSP and the high oxygen anisotropic atomic displacement value in the ZnO wurtzite crystal, which can lower the free energies for both H_2 and CO generation and accelerate the adsorption of reactant CO_2 molecules near the active sites. More interestingly, the interior of the flame-made nanoparticles was observed to consist of ZnO {101} facets, while the edges consist of {110} facets, as shown in **Figure 9b**. With increasing precursor flow rate, the ZnO nanoparticles preferentially grew along the <101> directions and exposed more {110} facets. The exposed {110} facets decreased the free energy barrier for formation of intermediates, and improved selectivity to the desired products, eventually achieving a H_2/CO ratio approaching 1.

Another related study produced a SnO_2 nanocatalyst for the reduction of CO_2 to formate [118], indicating that the particle size and surface area did not have a significant effect on electrocatalytic performance, but that surface defects governed the production rate and formate selectivity. Generally, the CO_2 molecules were initially adsorbed on surface defects and subsequently converted to formate on SnO_2 active sites. The presence of oxygen hole centers increased the charge density and the valence band maximum, which improved CO_2 activation and thus gave higher CO_2 conversion at low overpotential. The synthetic control of process parameters (e.g., increased precursor feed rate to reduce surface oxygen species due to incomplete combustion) was conducive to optimal surface defect density, achieving the highest electrocatalytic performance of 85% conversion to formate with a current density of −23.7 mA cm^{-2} at −1.1 V overpotential.

In addition, some studies of flame-synthesized electrocatalysts focused on the fabrication of perovskites because the flame process provides relatively high surface area while preventing the blocking of A-site ions. A previous report provided theoretical guidance for flame-made perovskite nanocatalysts and showed that $SrRuO_3$ and $LaRuO_3$ could provide high oxygen evolution reaction (OER) activity but poor thermodynamic stability in aqueous solutions [119]. Thus, recent studies highlight the incorporation of Fe in B-sites of such materials to improve thermodynamic stability. One of them prepared a Fe-doped double perovskite $PrBaCo_{2(1-x)}Fe_{2x}O_{6-\delta}$ catalyst, showing that the degradation of Co during OER was inhibited by Fe addition [120]. Also, the synergy between Fe and Co improved the electrocatalytic activity for the OER. But another study indicated that the incorporation of too much Fe in $LaCoO_3$ perovskite would decrease the OER activity [121]. With less Fe doping, the $LaCo_xFe_{1-x}O_3$ electrocatalyst showed a higher OER activity, with a current

density of 10 mA cm^{-2} at 1.64 V potential. An additional 40 mV overpotential was required to reach the same current density when the Fe content increased to 60%. A similar trend was also observed in electrocatalytic ethanol (EtOH) oxidation.

Although less research has been reported on the flame aerosol synthesis of electrocatalysts, we believe there is great potential in this field. So far, almost all of the flame-synthesized catalysts are metal-based. Some studies have revealed the potential of preparing conductive carbonaceous materials *via* flame aerosol processing [74, 122-124], but little attention has been given to flame synthesized carbon-based or carbon-covered electrocatalysts. This would be a good direction for further exploration.

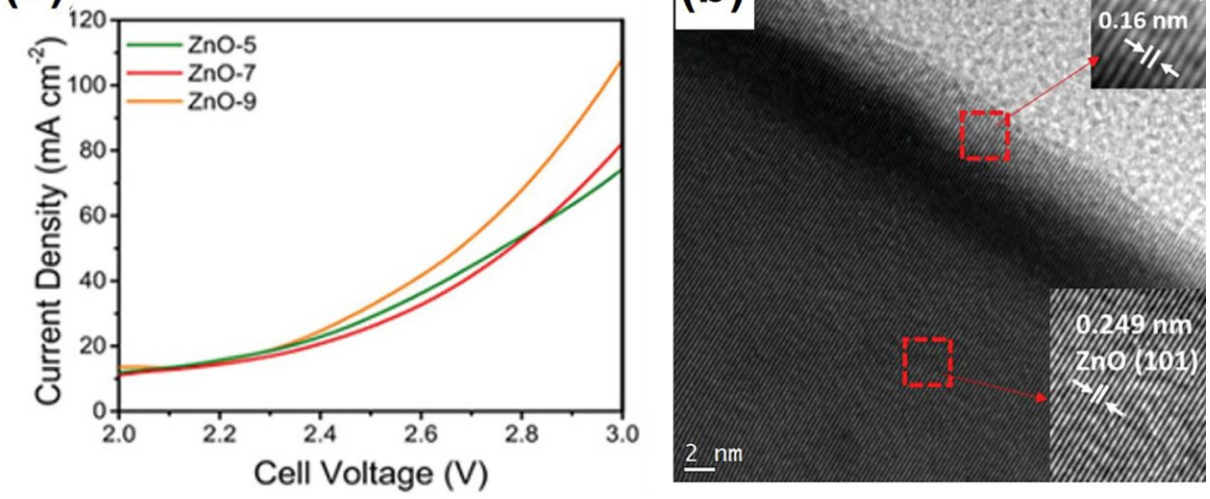

Figure 9. (a) Linear sweep voltammetry of ZnO electrocatalysts prepared with precursor feed rates of 5, 7, and 9 ml min^{-1}. **(b)** HR-TEM image of FSP-made ZnO electrocatalyst; Reproduced from ref. [117] with permission from Wiley-Blackwell.

5. Summary and outlook

Flame aerosol processing, the most common technology for large-scale industrial production of nanomaterials, has been widely explored to design catalysts in the past twenty years. Many studies have demonstrated that the flame aerosol processing could provide valuable opportunities for the synthesis of unique nanocatalysts, which are not accessible by traditional wet chemistry methods. Generally, flame aerosol processing provides flexibility for tailoring catalyst characteristics by controlling process parameters, leading to the rational design of catalysts towards desirable structure and function. The few and continuous manufacturing steps can enable scalable production with consistent physicochemical properties. However, some challenges still exist in this technology. To date, the vast majority of flame-made catalysts utilize the FSP reactor. The utilization of expensive organic precursor solvent increases production cost, while the FASP reactor uses less expensive aqueous precursors but often results in inhomogeneous particles. The production of non-porous and less crystalline nanoparticles also limits its application in some cases. To solve these problems, we should not only focus on the final catalytic performance for a particular reaction. More studies and *in situ* characterization efforts should be directed towards understanding the catalyst formation process during flame aerosol processing, and more advanced flame reactors must be developed.

In the past three years, more than 40 novel nanocatalysts were synthesized *via* flame aerosol processing. Most of them focus on environmental and energy issues, such as CO_2 utilization, CO oxidation, and H_2 production. These will remain hot topics in the foreseeable future. On the other hand, nearly all of the flame-made nanocatalysts were in the form of small nano-actives deposited on larger metal oxide (or silica) nanosphere

supports. Most efforts were devoted to optimizing catalytic activity by improving the surface area, dispersion, or doping with other elements to produce synergistic effects. However, while a noticeable advance could be seen in linking material characterization and catalytic mechanisms, the exploration of novel structures (like torus g-C_3N_4 and single Pd atoms) was limited. We believe that plenty of opportunities remain in the synthesis of unconventional structural, monoatomic, metal-free, or even porous nanocatalysts by flame aerosol processing.

Finally, beyond catalysis, flame aerosol processing also has great applications in other rapidly-growing fields, like sensors [125], electrode materials [126], photo-anodes [127], and bioimaging [128]. These materials and applications are considered in other review papers [45, 129, 130]. With respect to future applications beyond catalysis, we believe that application of flame aerosol made perovskite in solar cells is a promising direction for future research. Also, flame aerosol processing enables production of high purity and low toxicity materials with adjustable surface groups, so flame-made hollow silica and alumina microspheres may serve as carriers for targeted drug delivery and release. For such bio-applications, developing appropriately-certified manufacturing practices will be essential to clinical translation. In conclusion, early studies of flame aerosol processing mainly focused on industrial production of low-cost particles of simple oxides. However, greater attention is now being focused on its ability to prepare high-performance multi-component materials. In the future, we believe that flame aerosol processing will become an essential method for scalable fabrication of advanced nanomaterials for application in many fields, and that production of catalytic nanomaterials can play a leading role in this expansion of the importance of flame-made nanomaterials.

Acknowledgments

This work was partially supported by the National Science Foundation (grant CBET-1804996).

Conflicts of Interest

There are no conflicts of interest to declare.

References

[1] Y. Song, E. Ozdemir, S. Ramesh, A. Adishev, S. Subramanian, A. Harale, M. Albuali, B.A. Fadhel, A. Jamal, D.J.S. Moon, Dry reforming of methane by stable Ni–Mo nanocatalysts on single-crystalline MgO, Science, 367 (2020) 777-781.

[2] W.J. Stark, S.E. Pratsinis, Aerosol flame reactors for manufacture of nanoparticles, Powder Technol., 126 (2002) 103-108.

[3] G.D. Ulrich, Flame synthesis of fine particles, Chem. Eng. News, 62 (1984) 22-29.

[4] D.S. Ensor, Aerosol science and technology: History and reviews, 2011.

[5] K. Wegner, S.E. Pratsinis, Scale-up of nanoparticle synthesis in diffusion flame reactors, Chem. Eng. Sci., 58 (2003) 4581-4589.

[6] Karsten Wegner, Björn Schimmoeller, Bénédicte Thiebaut, Claudio Fernandez, T.N. Rao, Pilot Plants for Industrial Nanoparticle Production by Flame Spray Pyrolysis, KONA Powder Part. J., 29 (2011) 251-265.

[7] A.J. Grohn, S.E. Pratsinis, A. Sanchez-Ferrer, R. Mezzenga, K. Wegner, Scale-up of Nanoparticle Synthesis by Flame Spray Pyrolysis: The High-Temperature Particle Residence Time, Ind. Eng. Chem. Res., 53 (2014) 10734-10742.

[8] A. Heel, P. Holtappels, P. Hug, T. Graule, Flame Spray Synthesis of Nanoscale $La_{0.6}Sr_{0.4}Co_{0.2}Fe_{0.8}O_{3-\delta}$ and $Ba_{0.5}Sr_{0.5}Co_{0.8}Fe_{0.2}O_{3-\delta}$ as Cathode Materials for Intermediate Temperature Solid Oxide Fuel Cells, Fuel Cells, 10 (2010) 419-432.

[9] W. Stark, K. Wegner, S. Pratsinis, A. Baiker, Flame Synthesis of Vanadia/Titania Nano-particles for NO Removal, Part. Part. Syst. Charact., 19 (2002) 306-311.

[10] W.Y. Teoh, R. Amal, L. Mädler, Flame spray pyrolysis: An enabling technology for nanoparticles design and fabrication, Nanoscale, 2 (2010) 1324-1347.

[11] S.E. Pratsinis, Flame aerosol synthesis of ceramic powders, Prog. Energy Combust. Sci., 24 (1998) 197-220.

[12] C.B. Almquist, P. Biswas, Role of synthesis method and particle size of nanostructured TiO_2 on its photoactivity, J. Catal., 212 (2002) 145-156.

[13] J.-D. Grunwaldt, C. Beck, W. Stark, A. Hagen, A. Baiker, In situ XANES study on TiO_2–SiO_2 aerogels and flame made materials, Phys. Chem. Chem. Phys., 4 (2002) 3514-3521.

[14] J.R. Jensen, T. Johannessen, S. Wedel, H. Livbjerg, A study of $Cu/ZnO/Al_2O_3$ methanol catalysts prepared by flame combustion synthesis, J. Catal., 218 (2003) 67-77.

[15] B.S. Marshall, I. Telford, R. wood, A Field Method for the Determination of Zinc Oxide Fume in Air, 96 (1971) 569-578.

[16] R. Giacomuzzi, M. Portinari, I. Rossetti, L. Formi, A new method for preparing nanometer-size perovskitic catalysts for CH_4 flameless combustion, Stud. Surf. Sci. Catal., 130 (2000) 197-202.

[17] I. Rossetti, L. Forni, Catalytic flameless combustion of methane over perovskites prepared by flame-hydrolysis, Appl. Catal. B-Environ., 33 (2001) 345-352.

[18] E. Campagnoli, A. Tavares, L. Fabbrini, I. Rossetti, Y.A. Dubitsky, A. Zaopo, L. Forni, Effect of preparation method on activity and stability of $LaMnO_3$ and $LaCoO_3$ catalysts for the flameless combustion of methane, Appl. Catal. B-Environ., 55 (2005) 133-139.

[19] M. Sokolowski, A. Sokolowska, A. Michalski, B. Gokieli, The “in-flame-reaction” method for Al_2O_3 aerosol formation, J. Aerosol Sci., 8 (1977) 219-230.

[20] R. Mueller, L. Mädler, S.E. Pratsinis, Nanoparticle synthesis at high production rates by flame spray pyrolysis, Chem. Eng. Sci., 58 (2003) 1969-1976.

[21] R. Mueller, R. Jossen, S.E. Pratsinis, M. Watson, M.K. Akhtar, Zirconia nanoparticles made in spray flames at high production rates, J. Am. Ceram. Soc., 87 (2004) 197-202.

[22] M. Formenti, P. Vergnon, S.J. Teichner, P. Meriaudeau, F. Juillet, Preparation in a hydrogen-oxygen flame of ultrafine metal-oxide particles-oxidative properties toward hydrocarbons in presence of ultraviolet-radiation, J. Colloid Interface Sci., 39 (1972) 79-+.

[23] M.A. Fox, M.T. Dulay, Heterogeneous photocatalysis, Chem. Rev., 93 (1993) 341-357.

[24] T. Uematsu, S. Shimazu, T. Kameyama, K. Fukuda, New preparation methods for active superfine catalysts by spray reaction, Stud. Surf. Sci. Catal., 75 (1993) 1809-1812.

[25] R. Kriegel, J. Töpfer, N. Preuss, S. Grimm, J. Böer, Flame pyrolysis: A preparation route for ultrafine powders of metastable β-$SrMnO_3$ and $NiMn_2O_4$, J. Mater. Sci. Lett., 13 (1994) 1111-1113.

[26] P.F. Miquel, J.L. Katz, Flame synthesis of nanostructured vanadium oxide based catalysts, 1995.

[27] B. Schimmoeller, S.E. Pratsinis, A. Baiker, Flame aerosol synthesis of metal oxide catalysts with unprecedented structural and catalytic properties, Chemcatchem, 3 (2011) 1234-1256.

[28] B. Schimmoeller, H. Schulz, A. Ritter, A. Reitzmann, B. Kraushaar-Czarnetzki, A. Baiker, S. Pratsinis, Structure of flame-made vanadia/titania and catalytic behavior in the partial oxidation of o-xylene, J. Catal., 256 (2008) 74-83.

[29] W.J. Stark, K. Wegner, S.E. Pratsinis, A. Baiker, Flame aerosol synthesis of vanadia–titania nanoparticles: structural and catalytic properties in the selective catalytic reduction of NO by NH_3, J. Catal., 197 (2001) 182-191.

[30] K. Wegner, S.E. Pratsinis, Nozzle-quenching process for controlled flame synthesis of titania nanoparticles, AIChE J., 49 (2003) 1667-1675.

[31] I. Rossetti, L. Fabbrini, N. Ballarini, C. Oliva, F. Cavani, A. Cericola, B. Bonelli, M. Piumetti, E. Garrone, H. Dyrbeck, V_2O_5–SiO_2 systems prepared by flame pyrolysis as catalysts for the oxidative dehydrogenation of propane, J. Catal., 256 (2008) 45-61.

[32] B. Schimmoeller, Y. Jiang, S.E. Pratsinis, A. Baiker, Structure of flame-made vanadia/silica and catalytic behavior in the oxidative dehydrogenation of propane, J. Catal., 274 (2010) 64-75.

[33] S.E. Pratsinis, W. Zhu, S. Vemury, The role of gas mixing in flame synthesis of titania powders, Powder Technol., 86 (1996) 87-93.

[34] S. Wagloehner, M. Nitzer-Noski, S. Kureti, Oxidation of soot on manganese oxide catalysts, Chem. Eng. J., 259 (2015) 492-504.

[35] R. Strobel, M. Maciejewski, S.E. Pratsinis, A. Baiker, Unprecedented formation of metastable monoclinic $BaCO_3$ nanoparticles, Thermochim. Acta, 445 (2006) 23-26.

[36] S. Grimm, M. Schultz, S. Barth, R. Muller, Flame pyrolysis–a preparation route for ultrafine pure γ-Fe_2O_3 powders and the control of their particle size and properties, J. Mater. Sci., 32 (1997) 1083-1092.

[37] K. Schuh, W. Kleist, M. Høj, V. Trouillet, A.D. Jensen, J.-D. Grunwaldt, One-step synthesis of bismuth molybdate catalysts via flame spray pyrolysis for the selective oxidation of propylene to acrolein, Chem. Commun., 50 (2014) 15404-15406.

[38] T. Hirano, S. Nakakura, F.G. Rinaldi, E. Tanabe, W.N. Wang, T. Ogi, Synthesis of highly crystalline hexagonal cesium tungsten bronze nanoparticles by flame-assisted spray pyrolysis, Adv. Powder Technol., 29 (2018) 2512-2520.

[39] J. Yu, Z. Zhang, F. Dallmann, J. Zhang, D. Miao, H. Xu, A. Goldbach, R. Dittmeyer, Facile synthesis of highly active Rh/Al_2O_3 steam reforming catalysts with preformed support by flame spray pyrolysis, Appl. Catal. B-Environ., 198 (2016) 171-179.

[40] A. Tricoli, M. Graf, S.E. Pratsinis, Optimal doping for enhanced SnO_2 sensitivity and thermal stability, Adv. Funct. Mater., 18 (2008) 1969-1976.

[41] R. Koirala, S.E. Pratsinis, A. Baiker, Synthesis of catalytic materials in flames: opportunities and challenges, Chem. Soc. Rev., 45 (2016) 3053-3068.

[42] Y. Sheng, M. Kraft, R. Xu, Emerging applications of nanocatalysts synthesized by flame aerosol processes, Curr. Opin. Chem. Eng., 20 (2018) 39-49.

[43] R. Strobel, A. Baiker, S.E. Pratsinis, Aerosol flame synthesis of catalysts, Adv. Powder Technol., 17 (2006) 457-480.

[44] D.P. Debecker, S. Le Bras, C. Boissiere, A. Chaumonnot, C. Sanchez, Aerosol processing: a wind of innovation in the field of advanced heterogeneous catalysts, Chem. Soc. Rev., 47 (2018) 4112-4155.

[45] R. Strobel, S.E. Pratsinis, Flame aerosol synthesis of smart nanostructured materials, J. Mater. Chem., 17 (2007) 4743-4756.

[46] R. Strobel, F. Krumeich, W.J. Stark, S.E. Pratsinis, A. Baiker, Flame spray synthesis of Pd/Al_2O_3 catalysts and their behavior in enantioselective hydrogenation, J. Catal., 222 (2004) 307-314.

[47] M.K. Sharma, D. Qi, R.D. Buchner, W.J. Scharmach, V. Papavassiliou, M.T. Swihart, Flame-driven Aerosol Synthesis of Copper-Nickel Nanopowders and Conductive Nanoparticle Films, ACS Appl. Mater. Interfaces, 6 (2014) 13542-13551.

[48] A.J. Gröhn, S.E. Pratsinis, K. Wegner, Fluid-particle dynamics during combustion spray aerosol synthesis of ZrO_2, Chem. Eng. J., 191 (2012) 491-502.

[49] E.C. Lovell, J. Scott, R. Amal, Ni-SiO2 catalysts for the carbon dioxide reforming of methane: varying support properties by flame spray pyrolysis, Molecules, 20 (2015) 4594-4609.

[50] H. Li, S. Pokhrel, M. Schowalter, A. Rosenauer, J. Kiefer, L. Mädler, The gas-phase formation of tin dioxide nanoparticles in single droplet combustion and flame spray pyrolysis, Combust. Flame, 215 (2020) 389-400.

[51] R. Koirala, O.V. Safonova, S.E. Pratsinis, A. Baiker, Effect of cobalt loading on structure and catalytic behavior of CoO_x/SiO_2 in CO_2 -assisted dehydrogenation of ethane, Appl. Catal. A-Gen., 552 (2018) 77-85.

[52] F. Zhang, C. Kang, Y. Wei, H. Li, Aerosol-spraying synthesis of periodic mesoporous organometal silica spheres with chamber cavities as sctive and reusable catalysts in aqueous organic reactions, Adv. Funct. Mater., 21 (2011) 3189-3197.

[53] K.B. Riad, P.M. Wood-Adams, K. Wegner, Flame-made TiO_2 (B), Mater. Res. Bull., 106 (2018) 276-281.

[54] K. Fujiwara, Y. Deligiannakis, C.G. Skoutelis, S.E. Pratsinis, Visible-light active black TiO_2-Ag/TiO_x particles, Applied Catalysis B: Environmental, 154 (2014) 9-15.

[55] A. Teleki, N. Bjelobrk, S. Pratsinis, Flame-made Nb- and Cu-doped TiO_2 sensors for CO and ethanol, Sensors and Actuators B: Chemical, 130 (2008) 449-457.

[56] Y. Jiang, J. Scott, R. Amal, Exploring the relationship between surface structure and photocatalytic activity of flame-made TiO_2-based catalysts, Applied Catalysis B: Environmental, 126 (2012) 290-297.

[57] J. Huo, Y. Hu, H. Jiang, X. Hou, C. Li, Continuous flame synthesis of near surface nitrogen doped TiO_2 for dye-sensitized solar cells, Chem. Eng. J., 258 (2014) 163-170.

[58] P.G. Smirniotis, T. Boningari, D. Damma, S.N.R. Inturi, Single-step rapid aerosol synthesis of N-doped TiO_2 for enhanced visible light photocatalytic activity, Catal. Commun., 113 (2018) 1-5.

[59] I. Papailias, N. Todorova, T. Giannakopoulou, N. Ioannidis, P. Dallas, D. Dimotikali, C. Trapalis, Novel torus shaped g-C_3N_4 photocatalysts, Applied Catalysis B: Environmental, 268 (2020).

[60] F. Zhao, S. Li, X. Wu, R. Yue, W. Li, Y. Chen, Synergetic effect over flame-made manganese doped CuO–CeO_2 nanocatalyst for enhanced CO oxidation performance, RSC Advances, 9 (2019) 2343-2352.

[61] C.R. Bickmore, K.F. Waldner, D.R. Treadwell, R.M. Laine, Ultrafine spinel powders by flame spray pyrolysis of a magnesium aluminum double alkoxide, J. Am. Ceram. Soc., 79 (1996) 1419-1423.

[62] S. Thybo, S. Jensen, J. Johansen, T. Johannessen, O. Hansen, U. Quaade, Flame spray deposition of porous catalysts on surfaces and in microsystems, J. Catal., 223 (2004) 271-277.

[63] R.N. Grass, W.J. Stark, Gas phase synthesis of fcc-cobalt nanoparticles, J. Mater. Chem., 16 (2006) 1825-1830.

[64] A. Teleki, M.C. Heine, F. Krumeich, M.K. Akhtar, S.E. Pratsinis, In situ coating of flame-made TiO_2 particles with nanothin SiO_2 films, Langmuir, 24 (2008) 12553-12558.

[65] R. Strobel, L. Mädler, M. Piacentini, M. Maciejewski, A. Baiker, S.E. Pratsinis, Two-nozzle flame synthesis of Pt/Ba/Al_2O_3 for NOx storage, Chem. Mater., 18 (2006) 2532-2537.

[66] R. Buechel, S.E. Pratsinis, A. Baiker, Influence of controlled spatial deposition of Pt and Pd in NO_x storage-reduction catalysts on their efficiency, Appl. Catal. B-Environ., 101 (2011) 682-689.

[67] M. Tepluchin, D.K. Pham, M. Casapu, L. Mädler, S. Kureti, J.-D. Grunwaldt, Influence of single- and double-flame spray pyrolysis on the structure of MnO_x/γ-Al_2O_3 and FeO_x/γ-Al_2O_3 catalysts and their behaviour in CO removal under lean exhaust gas conditions, Catal. Sci. Technol., 5 (2015) 455-464.

[68] M. Høj, D.K. Pham, M. Brorson, L. Mädler, A.D. Jensen, J.-D. Grunwaldt, Two-nozzle flame spray pyrolysis (FSP) synthesis of CoMo/Al_2O_3 hydrotreating catalysts, Catal. Lett., 143 (2013) 386-394.

[69] J.A.H. Dreyer, H.K. Grossmann, J. Chen, T. Grieb, B.B. Gong, P.H.L. Sit, L. Mädler, W.Y. Teoh, Preferential oxidation of carbon monoxide over Pt–FeO /CeO_2 synthesized by two-nozzle flame spray pyrolysis, J. Catal., 329 (2015) 248-261.

[70] W.J. Scharmach, R.D. Buchner, V. Papavassiliou, P. Pacouloute, M.T. Swihart, A High-Temperature Reducing Jet Reactor for Flame-Based Metal Nanoparticle Production, Aerosol Sci. Technol., 44 (2010) 1083-1088.

[71] M.M. Mohammadi, S.S. Gunturi, S. Shao, S. Konda, R.D. Buchner, M.T. Swihart, Flame-synthesized nickel-silver nanoparticle inks provide high conductivity without sintering, Chem. Eng. J., 372 (2019) 648-655.

[72] S. Konda, M.M. Mohammadi, R.D. Buchner, H.Q. Lin, M.T. Swihart, Flame-based synthesis and in situ functionalization of palladium alloy nanoparticles, AIChE J., 64 (2018) 3826-3834.

[73] Mohammad Moein Mohammadi, Naveshkaanth Alexander, Anirudh Raghavan, William Sullivan, Raymond Buchner, Haiqing Lin, Carl RF Lund, M.T. Swihart, Catalyst Design and Production for Methane Dry Reforming Using a Flame-Driven High Temperature Reducing Jet Aerosol Reactor, 2019 AIChE Annual Meeting, (2019).

[74] M.M. Mohammadi, S. Shao, S. Srivatsa Gunturi, A.R. Raghavan, N. Alexander, Y. Liu, C.M. Stafford, R.D. Buchner, M.T. Swihart, A general approach to multicomponent metal-decorated crumpled reduced graphene oxide nanocomposites using a flame-based process, Nanoscale, 11 (2019) 19571-19578.

[75] J. Tollefson, CO_2 emissions set to spike in 2017, Nature, 551 (2017) 283-283.

[76] K.D. Kim, S. Pokhrel, Z. Wang, H. Ling, C. Zhou, Z. Liu, M. Hunger, L. Maedler, J. Huang, Tailoring High-Performance Pd Catalysts for Chemoselective Hydrogenation Reactions via Optimizing the Parameters of the Double-Flame Spray Pyrolysis, ACS Catal., 6 (2016) 2372-2381.

[77] J.A.H. Dreyer, P. Li, L. Zhang, G.K. Beh, R. Zhang, P.H.L. Sit, W.Y. Teoh, Influence of the oxide support reducibility on the CO_2 methanation over Ru-based catalysts, Appl. Catal. B-Environ., 219 (2017) 715-726.

[78] S. Tada, K. Fujiwara, T. Yamamura, M. Nishijima, S. Uchida, R. Kikuchi, Flame spray pyrolysis makes highly loaded Cu nanoparticles on ZrO_2 for CO_2-to-methanol hydrogenation, Chem. Eng. J., 381 (2020).

[79] K. Fujiwara, S. Tada, T. Honma, H. Sasaki, M. Nishijima, R. Kikuchi, Influences of particle size and crystallinity of highly loaded CuO/ZrO_2 on CO_2 hydrogenation to methanol, AIChE J., 65 (2019).

[80] S. Tada, K. Larmier, R. Büchel, C. Copéret, Methanol synthesis via CO_2 hydrogenation over CuO–ZrO2 prepared by two-nozzle flame spray pyrolysis, Catal. Sci. Technol., 8 (2018) 2056-2060.

[81] J. Horlyck, M. Sara, E.C. Lovell, R. Amal, J. Scott, Effect of Metal‐Support Interactions in Mixed Co/Al Catalysts for Dry Reforming of Methane, ChemCatChem, 11 (2019) 3432-3440.

[82] J. Horlyck, S. Pokhrel, E. Lovell, N.M. Bedford, L. Mädler, R. Amal, J. Scott, Unifying double flame spray pyrolysis with lanthanum doping to restrict cobalt–aluminate formation in Co/Al_2O_3 catalysts for the dry reforming of methane, Catal. Sci. Technol., 9 (2019) 4970-4980.

[83] J. Horlyck, S. Lewis, R. Amal, J. Scott, The Impact of La Doping on Dry Reforming Ni-Based Catalysts Loaded on FSP-Alumina, Top. Catal., 61 (2018) 1842-1855.

[84] P. Demokritou, R. Buchel, R.M. Molina, G.M. Deloid, J.D. Brain, S.E. Pratsinis, Development and characterization of a Versatile Engineered Nanomaterial Generation System (VENGES) suitable for toxicological studies, Inhal. Toxicol., 22 (2010) 107-116.

[85] A. Spyrogianni, I.K. Herrmann, K. Keevend, S.E. Pratsinis, K. Wegner, The silanol content and in vitro cytolytic activity of flame-made silica, J. Colloid Interface Sci., 507 (2017) 95-106.

[86] E.C. Lovell, H. Grossman, J. Horlyck, J. Scott, L. Mädler, R. Amal, Asymmetrical Double Flame Spray Pyrolysis-Designed $SiO_2/Ce_{0.7}Zr_{0.3}O_2$ for the Dry Reforming of Methane, ACS Appl. Mater. Interfaces, 11 (2019) 25766-25777.

[87] E. Ogel, M. Casapu, D.E. Doronkin, R. Popescu, H. Störmer, C. Mechler, G. Marzun, S. Barcikowski, M. Türk, J.D. Grunwaldt, Impact of Preparation Method and Hydrothermal Aging on Particle Size Distribution of $Pt/\gamma\text{-}Al_2O_3$ and Its Performance in CO and NO Oxidation, J. Phys. Chem. C, 123 (2019) 5433-5446.

[88] X. Zhao, Y. Hu, H. Jiang, J. Yu, R. Jiang, C. Li, Engineering TiO_2 supported Pt sub-nanoclusters via introducing variable valence Co ion in high-temperature flame for CO oxidation, Nanoscale, 10 (2018) 13384-13392.

[89] W. Bi, Y. Hu, H. Jiang, H. Yu, W. Li, C. Li, In-situ synthesized surface N-doped Pt/TiO_2 via flame spray pyrolysis with enhanced thermal stability for CO catalytic oxidation, Appl. Surf. Sci., 481 (2019) 360-368.

[90] X. Chen, Z. Xu, F. Yang, H. Zhao, Flame spray pyrolysis synthesized $CuO\text{-}TiO_2$ nanoparticles for catalytic combustion of lean CO, Proc. Combust. Inst., 37 (2019) 5499-5506.

[91] F. Zhao, S. Li, X. Wu, R. Yue, W. Li, X. Zha, Y. Deng, Y. Chen, Catalytic Behaviour of Flame-Made CuO-CeO2 Nanocatalysts in Efficient CO Oxidation, Catalysts, 9 (2019).

[92] K. Wegner, M. Medicus, E. Schade, J. Grothe, S. Kaskel, Tailoring Catalytic Properties of Copper Manganese Oxide Nanoparticles (Hopcalites-2G) via Flame Spray Pyrolysis, ChemCatChem, 10 (2018) 3914-3922.

[93] K. Wegner, R. Zippel, M. Medicus, E. Schade, J. Grothe, S. Kaskel, Molecular Precursors for Tailoring Humidity Tolerance of Nanoscale Hopcalite Catalysts Via Flame Spray Pyrolysis, ChemCatChem, 11 (2019) 4593-4603.

[94] K. Simmance, D. Thompsett, W. Wang, B. Thiebaut, Evaluation of perovskite catalysts prepared by flame spray pyrolysis for three-way catalyst activity under simulated gasoline exhaust feeds, Catal. Today, 320 (2019) 40-50.

[95] S. Angel, J. Neises, M. Dreyer, K. Friedel Ortega, M. Behrens, Y. Wang, H. Arandiyan, C. Schulz, H. Wiggers, Spray-flame synthesis of $La(Fe, Co)O_3$ nano-perovskites from metal nitrates, AIChE J., 66 (2019).

[96] N. Wang, F. Niu, S. Wang, Y. Huang, Catalytic activity of flame-synthesized Pd/TiO_2 for the methane oxidation following hydrogen pretreatments, Particuology, 41 (2018) 58-64.

[97] L. Meng, H. Zhao, Low-temperature complete removal of toluene over highly active nanoparticles $CuO\text{-}TiO_2$ synthesized via flame spray pyrolysis, Appl. Catal. B-Environ., 264 (2020).

[98] B. Xu, L. Dong, Y. Chen, Influence of CuO loading on dispersion and reduction behavior of CuO/TiO_2 (anatase) system, J. Chem. Soc., Faraday Trans., 94 (1998) 1905-1909.

[99] Y.-J. Wang, C. Liu, Y.-J. Wu, Y.-H. Song, M.-L. Zhu, J. Huang, Z.-T. Liu, Z.-W. Liu, Flame-spray-pyrolysis amorphous alumina-silica for tailoring the product distribution of Fischer-Tropsch synthesis, Catal. Today, 339 (2020) 40-47.

[100] P. Sprenger, T. Sheppard, J.-P. Suuronen, A. Gaur, F. Benzi, J.-D. Grunwaldt, Structural Evolution of Highly Active Multicomponent Catalysts for Selective Propylene Oxidation, Catalysts, 8 (2018).

[101] B. Pongthawornsakun, O. Mekasuwandumrong, F.J.C. Santos Aires, R. Büchel, A. Baiker, S.E. Pratsinis, J. Panpranot, Variability of particle configurations achievable by 2-nozzle flame syntheses of the $Au\text{-}Pd\text{-}TiO_2$ system and their catalytic behaviors in the selective hydrogenation of acetylene, Appl. Catal. A-Gen., 549 (2018) 1-7.

[102] L. Gavilà, A. Lähde, J. Jokiniemi, M. Constanti, F. Medina, E. Río, D. Tichit, M.G. Álvarez, Insights on the One-Pot Formation of 1,5-Pentanediol from Furfural with Co−Al Spinel-based Nanoparticles as an Alternative to Noble Metal Catalysts, ChemCatChem, 11 (2019) 4944-4953.

[103] G.K. ACS Appl Mater InterfacesBeh, C.T. Wang, K. Kim, J. Qu, J. Cairney, Y.H. Ng, A.K. An, R. Ryoo, A. Urakawa, W.Y. Teoh, Flame-made amorphous solid acids with tunable acidity for the aqueous conversion of glucose to levulinic acid, Green Chem., 22 (2020) 688-698.

[104] Y.K. Kho, A. Iwase, W.Y. Teoh, L. Mädler, A. Kudo, R. Amal, Photocatalytic H_2 evolution over TiO_2 nanoparticles. The synergistic effect of anatase and rutile, J. Phys. Chem. C, 114 (2010) 2821-2829.

[105] E. Bahadori, A. Tripodi, G. Ramis, I. Rossetti, Semi-Batch Photocatalytic Reduction of Nitrates: Role of Process Conditions and Co-Catalysts, ChemCatChem, 11 (2019) 4642-4652.

[106] G.L. Chiarello, D. Ferri, E. Selli, In situ attenuated total reflection infrared spectroscopy study of the photocatalytic steam reforming of methanol on Pt/TiO_2, Appl. Surf. Sci., 450 (2018) 146-154.

[107] K. Fujiwara, S.E. Pratsinis, Single Pd atoms on TiO2 dominate photocatalytic NO_x removal, Appl. Catal. B-Environ., 226 (2018) 127-134.

[108] F. Mikaeili, S. Topcu, G. Jodhani, P.-I. Gouma, Flame-Sprayed Pure and Ce-Doped TiO_2 Photocatalysts, Catalysts, 8 (2018).

[109] Z. Wang, Y. Liu, D.J. Martin, W. Wang, J. Tang, W. Huang, CuO_x–TiO_2 junction: what is the active component for photocatalytic H_2 production?, Phys. Chem. Chem. Phys., 15 (2013) 14956-14960.

[110] F. Yang, M. Liu, X. Chen, Z. Xu, H. Zhao, Simultaneous Control over Lattice Doping and Nanocluster Modification of a Hybrid CuO_x/TiO_2 photocatalyst during Flame Synthesis for Enhancing Hydrogen Evolution, Sol. RRL, 2 (2018).

[111] T. Boningari, S.N.R. Inturi, M. Suidan, P.G. Smirniotis, Novel one-step synthesis of sulfur doped-TiO_2 by flame spray pyrolysis for visible light photocatalytic degradation of acetaldehyde, Chem. Eng. J., 339 (2018) 249-258.

[112] T. Boningari, S.N.R. Inturi, M. Suidan, P.G. Smirniotis, Novel one-step synthesis of nitrogen-doped TiO_2 by flame aerosol technique for visible-light photocatalysis: Effect of synthesis parameters and secondary nitrogen (N) source, Chem. Eng. J., 350 (2018) 324-334.

[113] C. Ma, X. Zou, H. Li, A. Li, Z. Gao, L. Zhu, Z. Huang, Flame synthesized MoO_3 nanobelts and nanoparticles coated with $BiVO_4$ for photoelectrochemical hydrogen production, Energy Conv. Manag., 205 (2020).

[114] O. Arutanti, A.F. Arif, R. Balgis, T. Ogi, K. Okuyama, F. Iskandar, Tailored synthesis of macroporous Pt/WO_3 photocatalyst with nanoaggregates via flame assisted spray pyrolysis, AIChE J., 62 (2016) 3864-3873.

[115] G. Merle, M. Wessling, K. Nijmeijer, Anion exchange membranes for alkaline fuel cells: A review, J. Membr. Sci., 377 (2011) 1-35.

[116] X.X. Zou, Y. Zhang, Noble metal-free hydrogen evolution catalysts for water splitting, Chem. Soc. Rev., 44 (2015) 5148-5180.

[117] R. Daiyan, E.C. Lovell, B. Huang, M. Zubair, J. Leverett, Q. Zhang, S. Lim, J. Horlyck, J. Tang, X. Lu, K. Kalantar-Zadeh, J.N. Hart, N.M. Bedford, R. Amal, Uncovering Atomic-Scale Stability and Reactivity in Engineered Zinc Oxide Electrocatalysts for Controllable Syngas Production, Adv. Energy Mater., (2020).

[118] R. Daiyan, E.C. Lovell, N.M. Bedford, W.H. Saputera, K.H. Wu, S. Lim, J. Horlyck, Y.H. Ng, X. Lu, R. Amal, Modulating Activity through Defect Engineering of Tin Oxides for Electrochemical CO_2 Reduction, Adv. Sci., 6 (2019) 1900678.

[119] B.-J. Kim, D.F. Abbott, X. Cheng, E. Fabbri, M. Nachtegaal, F. Bozza, I.E. Castelli, D. Lebedev, R. Schaeublin, C. Coperet, T. Graule, N. Marzari, T.J. Schmidt, Unraveling Thermodynamics, Stability, and Oxygen Evolution Activity of Strontium Ruthenium Perovskite Oxide, ACS Catal., 7 (2017) 3245-3256.

[120] B.-J. Kim, E. Fabbri, I. Castelli, M. Borlaf, T. Graule, M. Nachtegaal, T. Schmidt, Fe-Doping in Double Perovskite $PrBaCo_{2(1-x)}Fe_{2x}O_{6-\delta}$: Insights into Structural and Electronic Effects to Enhance Oxygen Evolution Catalyst Stability, Catalysts, 9 (2019).

[121] B. Alkan, S. Cychy, S. Varhade, M. Muhler, C. Schulz, W. Schuhmann, H. Wiggers, C. Andronescu, Spray-Flame-Synthesized $LaCo_{1-x}Fe_xO_3$ Perovskite Nanoparticles as Electrocatalysts for Water and Ethanol Oxidation, ChemElectroChem, 6 (2019) 4266-4274.

[122] H. Lee, T.J. Kim, C. Li, I.D. Choi, Y.T. Kim, Z. Coker, T.Y. Choi, D. Lee, Flame aerosol synthesis of carbon-supported Pt-Ru catalysts for a fuel cell electrode, Int. J. Hydrogen Energy, 39 (2014) 14416-14420.

[123] Y.C. Liu, B.M. Sun, Z.Y. Ding, Influence analysis of sampling time for synthesis of carbon nanotubes in the V-type pyrolysis flame, Advanced Material Research, Trans Tech Publications Ltd, Durnten-Zurich, 2011, pp. 235-+.

[124] W.J. Scharmach, M.K. Sharma, R.D. Buchner, V. Papavassiliou, G.N. Vajani, M.T. Swihart, Amorphous Carbon Encapsulation of Metal Aerosol Nanoparticles for Improved Collection and Prevention of Oxidation, AIChE J., 59 (2013) 4116-4123.

[125] A. Sukee, A.A. Alharbi, A. Staerz, A. Wisitsoraat, C. Liewhiran, U. Weimar, N. Barsan, Effect of AgO loading on flame-made $LaFeO_3$ p-type semiconductor nanoparticles to acetylene sensing, Sens. Actuator B-Chem., 312 (2020).

[126] S.H. Choi, Y.C. Kang, One-pot facile synthesis of Janus-structured SnO_2-CuO composite nanorods and their application as anode materials in Li-ion batteries, Nanoscale, 5 (2013) 4662-4668.

[127] G.Y. Liu, S.K. Karuturi, H.J. Chen, L. Spiccia, H.H. Tan, C. Jagadish, D.W. Wang, A.N. Simonov, A. Tricoli, Tuning the morphology and structure of disordered hematite photoanodes for improved water oxidation: A physical and chemical synergistic approach, Nano Energy, 53 (2018) 745-752.

[128] G.A. Sotiriou, D. Franco, D. Poulikakos, A. Ferrari, Optically Stable Biocompatible Flame-Made SiO_2-Coated Y_2O_3: Tb^{3+} Nanophosphors for Cell Imaging, ACS Nano, 6 (2012) 3888-3897.

[129] H. Chen, H.K. Mulmudi, A. Tricoli, Flame spray pyrolysis for the one-step fabrication of transition metal oxide films: Recent progress in electrochemical and photoelectrochemical water splitting, Chin. Chem. Lett., 31 (2020) 601-604.

[130] J.A. Kemmler, S. Pokhrel, L. Mädler, U. Weimar, N. Barsan, Flame spray pyrolysis for sensing at the nanoscale, Nanotechnology, 24 (2013) 14.

Tables

Table 1. Thermal catalysts synthesized by flame aerosol processing in the past three years

Catalyst (Actives/Support)	Reactor type	Reaction	Structure			Optimal Catalytic Performance	Ref.
			Act. cont. (wt% or mol %)	Particle size (nm) (Actives/Support)	SSA (m^2 g^{-1})		
Ru/CeO_2	FSP	CO_2 hydrogenation to methane	5	1.6~7.1/NA	NA[a]	83% CO_2 conversion, 99% CH_4 selectivity at 300°C	[77]
Ru/MnO_x		CO_2 hydrogenation to methane	5	1.6~7.1/NA	NA	25% CO_2 conversion, 90% CH_4 selectivity at 300°C	
Ru/Al_2O_3		CO_2 hydrogenation to methane	5	1.6~7.1/NA	NA	32% CO_2 conversion, 94% CH_4 selectivity at 300°C	
Ru/ZnO		CO_2 hydrogenation to methane	5	1.6~7.1/NA	NA	1% CO_2 conversion, 6% CH_4 selectivity at 300°C	
Cu/ZrO_2	FSP	CO_2 hydrogenation to methanol	60	10~20/~10	62~235	2~4% CO_2 conversion, 50~60% methanol selectivity, methanol production rate 20 ml $h^{-1}g_{cat}^{-1}$ at 230°C	[78]
Cu/ZrO_2	FSP	CO_2 hydrogenation to methanol	60	12~17/3.7~7	NA	6~10% CO_2 conversion, 50~60% methanol selectivity, methanol production rate 30 ml $h^{-1}g_{cat}^{-1}$ at 230°C	[79]
Cu/ZrO_2	DFSP	CO_2 hydrogenation to methanol	11~14	<5 /~10	106~114	2~6 % CO_2 conversion, 45~60% methanol selectivity, methanol production rate 7 ml $min^{-1}g_{cu}^{-1}$ at 270°C	[80]
Co/Al_2O_3	FSP	Methane dry reforming	10~90	1~2/10~20	88~126	98% methane conversion, H_2:CO≈1.2 at 800°C; 78% methane conversion H_2:CO≈1.1 at 700°C	[81]
Co/Al_2O_3-La_2O_3	DFSP	Methane dry reforming	10	NA/5~30	111~122	96% methane conversion, H_2:CO≈1.02 at 800°C; 89% methane conversion H_2:CO≈0.9 at 700°C	[82]
Ni-Co/Al_2O_3-La_2O_3	FSP	Methane dry reforming	7.5-2.5	NA	NA	80% methane conversion, H_2:CO≈0.8 at 800°C; 50% methane conversion H_2:CO≈0.7 at 700°C	[83]
Ni/ SiO_2-$Ce_{0.7}Zr_{0.3}O_2$	DFSP	Methane dry reforming	10	10~15/9.5~12	141~276	73% methane conversion, H_2:CO≈0.98 at 800°C; 55% methane conversion H_2:CO≈0.8 at 700°C	[86]
Co/SiO_2	FSP	CO_2-assisted ethane dehydrogenation	0.3~4.5	1/NA	250~500	46% C_2H_2 conversion, 85% C_2H_4 selectivity at 700°C	[51]
Pt/Al_2O_3	FSP	CO oxidation; NO oxidation	2.2	1.8~7.7/NA	220	T_{50}[b]≈104°C, T_{100}≈108°C CO conversion; 70% NO conversion at 290°C	[87]
Pt/TiO_2	FSP	CO oxidation	1	2.47/5~25	64	T_{50}≈110°C, T_{100}≈120°C; CO reaction rate 0.13×10^{-7} mol s^{-1} g_{cat}^{-1}	[88]
Pt/TiO_2-Co		CO oxidation	1	0.72/5~25	60	T_{50}≈40°C, T_{100}≈70°C; CO reaction rate 5.46×10^{-7} mol s^{-1} g_{cat}^{-1}	
Pt/TiO_2	FSP	CO oxidation	1	1.2~5.45/NA	64	T_{100}≈100°C after 300°C calcination; T_{100}≈200°C after 600°C calcination;	[89]
Pt/TiO_2-N		CO oxidation	1	1.34~4.29/NA	61	T_{100}≈120°C after 300°C calcination; T_{100}≈150°C after 600°C calcination;	
CuO/TiO_2	FSP	CO oxidation	2~20	<4/15~20	70~98	T_{50}≈92°C, T_{100}≈120°C	[90]
CuO/CeO_2	FSP	CO oxidation	1~17	NA/25.6~32.8	39~54	T_{50}≈70°C, T_{100}≈120°C; keep 90% conversion for 23h at 1.7% water vapor condition	[91]
CuO/CeO_2-Mn	FSP	CO oxidation	15	NA/27~37	31~45	T_{50}≈93°C, T_{90}≈131°C; keep 100% conversion for 9h at 1.7% water vapor condition	[60]
Hopcalite	FSP	CO oxidation at humid atmosphere	Mn:Cu=2:1	5.2~5.7	133~193	Keep above 65% CO conversion for 1h in 75% humidity at 50°C	[92]
Hopcalite	FSP	CO oxidation at humid atmosphere	Mn:Cu=2.1:1	5~10	111~178	T_{90}≈90°C at dry condition; Keep above 50% CO conversion for 1h in 75% humidity at 50°C	[93]
$La_{1-x}A_xBO_3$	FSP	CO, NO, C_xH_y three-way oxidation	-	11~14	55~79	85% CO, 60% NO, 80% C_xH_y conversion at 500°C	[94]
$LaCoO_3$	FSP	CO oxidation	-	6.14~9.39	23~95	T_{100}≈175°C	[95]

Pd/TiO_2	FSP	Methane combustion	53	10	NA	Lowest light-off temperature 280°C; 85% methane conversion at 600°C	[96]
CuO/TiO_2	FSP	Toluene combustion	2~50	4/15~22	51~99	T_{50}=182°C, T_{90}=220°C; Keep above 90% toluene conversion for 10h at 250°C	[97]
Ru/SiO_2-Al_2O_3	FSP	Fischer-Tropsch synthesis	3	5.4~7/18~22	133~243	37% CO conversion at 240°C	[99]
Bi-Mo-Fe-Co oxide	FSP	Propylene oxidation to acrolein and acrylic acid	7.2-59.2-24.8-8.8	5~30	52	90% propylene conversion, around 40% acrolein and 50% acrylic acid selectivity at 330°C	[100]
Au-Pd/TiO_2	DFSP	Acetylene hydrogenation	Au 0.82 Pd 0.94	1~2/17	104	45% C_2H_2 conversion, 96% C_2H_4 selectivity at 40°C	[101]
Co-Al spinel	FSP	Furfural hydrogenation	Co:Al= 0.22:1	2.8~9	112~174	100% furfural conversion, 30% pentanediol, 60% tetrahydrofurfuryl alcohol selectivity at 150°C after 8h	[102]
SiO_2-Al_2O_3	FSP	Conversion of glucose to levulinic acid	0~100	4~9	180~478	100% glucose conversion, 40% levulinic acid selectivity at 180°C	[103]
SiO_2-Al_2O_3-Phosphate		Conversion of glucose to levulinic acid	0~100	6~35	58~268	100% glucose conversion, 42% levulinic acid selectivity at 180°C	

a.NA: Related data is not available; b. T_x: Arrive X% reactant conversion at T_x °C.

Table 2. Photocatalysts and electrocatalysts synthesized by flame aerosol processing in the past three years

Catalyst	Reactor type	Reaction	Structure			Optimal Catalytic Performance	Ref.
			Dop. cont. (wt% or mol%)	Particle size (nm)	SSA (m^2 g^{-1})		
Ag-TiO_2	FSP	Nitrate reduction	0.1	21	61	14.5% NO^{3-} conversion, 0.175mmol/h g_{cat} rate at 5.11 pH under 200W Hg light	[105]
Pt-TiO_2	FSP	Steam reforming methanol	0.5	1.3/10~25	70	NA	[106]
Pd-TiO_2	FSP	NO_x removal	0.1	-	87	80% NO conversion, 50% average NO_x removal efficiency in 5h under sunlight	[107]
Ce-TiO_2	FSP	Methylene blue degradation	24	5~45	NA	70% methylene blue degradation efficiency after 3h under 150W Xe lamp	[108]
CuO-TiO_2	FSP	Water splitting hydrogen	2	6~40	144	112.6 μmol h^{-1} H_2 production rate under 300W Xe lamp	[110]
S-TiO_2	FSP	Acetaldehyde degradation	0.18~0.38	122~311	4.8~12.3	60% acetaldehyde degradation under six F8T5 ww lamps	[111]
N-TiO_2	FSP	Phenol degradatoin	-	6~88	17~22	50% phenol degradation under six F8T5 ww lamps	[58]
N-TiO_2	FSP	Phenol degradation	0.5~7	42~88	16~26	50% phenol degradation under six F8T5 ww lamps	[112]
Pt-g-C_3N_4	FSP	Water splitting hydrogen	3	10~20	81.85	41.18 μmol g^{-1} h^{-1} H_2 production rate under 400 W R7S lamp	[59]
ZnO	FSP	CO_2 reduction	-	16.8~21.6	NA	Keep H2:CO≈1 with a current density of 40 mA cm^{-2} at 2.6V for 18h	[117]
SnO_2	FSP	CO_2 reduction	-	9~14	81~146	85% formate conversion with a current density of −23.7 mA cm^{-2} at −1.1 V	[118]
$PrBaCo_{2(1-x)}Fe_{2x}O_{6-\delta}$	FSP	Oxygen evolution reaction	-	5~30	43~56	50 mV dec^{-1} Tafel slope, 19.7 A g^{-1} current density at 1.55 V_{RHE}	[120]
$LaCo_{1-x}Fe_xO_3$	FSP	Oxygen evolution reaction	0~60 Fe	6~7	NA	10 mA cm^{-2} current density at 1.64 V	[121]
		EtOH oxidation				10 mA cm^{-2} current density at 1.58 V	